Journal of Marine Research, 58, 327–373, 2000

Journal of
MARINE RESEARCH

Volume 58, Number 3

A baroclinic western boundary current over a continental slope

Rupert Ford[1]

ABSTRACT

Baroclinic flow over a western continental slope is investigated using a simple model in which inertia is completely neglected and the temperature of the ocean depends only on horizontal position. Solutions of this model are also solutions of the three-dimensional equations without inertia. This model is arguably the simplest model in which the Joint Effect of Baroclinicity and Relief (JEBAR) can affect the mass transport on the slope. Offshore, we suppose that a classical double-gyre circulation exists, in which the subpolar gyre is colder than the subtropical gyre. Using asymptotic expansions based on small viscosity and small thermal diffusivity, we show analytically that a thin baroclinic current, or front, forms on the slope. The baroclinic current flows across the slope from south to north and shallow to deep. Recirculating gyres are formed on both flanks of the current, and the extent to which both the baroclinic current and the gyres resemble the observed flow in the Western North Atlantic is discussed.

1. Introduction

In the classic, flat-bottomed noninertial theories of wind-driven ocean circulation (Stommel, 1948; Munk, 1950) intense frictional boundary currents form along the entire length of the western boundary of the ocean. In these theories, the depth-integrated flow is independent of the stratification. On the other hand, if the fluid is barotropic, with uniform density, and the ocean depth vanishes at the coast, the streamlines for the depth-integrated flow follow contours of f/H, where f is the Coriolis parameter and H is the depth of the ocean (Holland, 1967). Boundary currents are intensified because contours of f/H come closer together on the slope than in the deep ocean, but frictional effects are confined to a

1. Department of Mathematics, Imperial College, 180 Queen's Gate, London, United Kingdom, SW7 2BZ.
email: r.ford@ic.ac.uk

southwestern corner region (Salmon, 1992). In this paper, we develop a simple model in which an intense baroclinic current flows over the continental slope, and whose width is controlled by friction.

There have been several previous attempts to understand baroclinic western boundary currents with topography. Predominantly, they have either been numerical (Holland, 1973; Salmon, 1994; Bryan *et al.,* 1995), the topography has been confined to unventilated layers (Welander, 1968; Liu, 1990; Thompson, 1995; Özgökmen *et al.,* 1997), or they have made some special assumptions about the structure of the flow (Salmon, 1992). In this paper, we adopt an alternative approach. We consider the simplest form of stratification permissible by three-dimensional geostrophic and hydrostatic dynamics, and we insist that our model has three important properties. Firstly, the three-dimensional evolution equations must be satisfied, even though the choice of stratification will reduce the degrees of freedom to two spatial dimensions. Secondly, forcing and friction must be consistent with the simple form of stratification that we choose, but they are otherwise arbitrary. Thirdly, the solutions must be consistent with circulation in a closed wind- and thermally-driven basin.

Under geostrophic hydrostatic dynamics the potential vorticity is $f\sigma_z$, where σ is the buoyancy. If $f\sigma_z = 0$ everywhere initially, then it must remain so for all time, because potential vorticity is conserved on fluid particles. Arguably the simplest form of stratification permissible by the three-dimensional dynamics is therefore $\sigma_z = 0$. That is, there are horizontal gradients of temperature, but not vertical ones. Indeed, one can see without considering the potential vorticity that this ansatz is preserved under adiabatic geostrophic evolution because the depth-dependent part of the horizontal velocity—the thermal wind—is tangent to the contours of constant temperature. Following Salmon (1994), effects of diffusion of momentum and of temperature are projected onto the assumption of a temperature field that is independent of depth. This is the simple model that we develop in this paper. These equations have been studied by Salmon and Ford (1995), but in that paper a further assumption was made relating the steamfunction and the temperature. In this paper we solve the following problem without any such additional assumptions.

We suppose that wind- and thermal-forcing in the deep ocean, east of the continental slope, establish a double-gyre circulation, with a cold cyclonic subpolar gyre, and a warm anticyclonic subtropical gyre. We suppose further that the viscosity ν and thermal diffusivity κ are both small. We develop solutions on the slope that match to these prescribed deep ocean conditions so that the entire solution is consistent with circulation in a closed wind- and thermally-driven basin. Two questions then arise. Firstly, under what conditions can a solution on the continental slope be found that matches to the solution in the deep ocean? Secondly, what is the structure of this solution, when it exists, and to what extent does it resemble features of observed western boundary currents?

The paper is organized as follows. In Section 2 we develop the equations and formulate the mathematical problem to be solved. In Section 3 we develop the linear theory, based on the assumption that the temperature difference $\mathscr{T}$ between the subpolar and subtropical gyres is small. In this limit the streamfunction is unaffected by the temperature at leading

order, and the temperature behaves as a passive tracer, advected around by the barotropic streamfunction. It is clear that a solution exists in this limit. We then compute the next-order correction to the streamfunction, and show that the linear analysis is valid only if $\mathscr{T} \ll O(\nu^{1/2})$, in an appropriate nondimensional sense. The relatively small magnitude of $\mathscr{T}$ required for validity of Section 3 suggests that the linear solution is not physically relevant, but the insight and mathematical formulation developed in this section are helpful later. In Section 4 a weakly-nonlinear analysis for $\mathscr{T} = O(\nu^{1/2})$ is presented, and we show how this is consistent with the linear analysis when $\mathscr{T}/\nu^{1/2} \to 0$, and with a fully nonlinear analysis in the limit $\mathscr{T}/\nu^{1/2} \to \infty$. The fully nonlinear analysis is presented in Section 5, and it is valid for $\mathscr{T} = O(1)$. However, we find that there is a maximum value of $\mathscr{T}$ above which our solution breaks down. We discuss this further in Section 6, and offer some concluding remarks.

2. Model equations and problem formulation

We take as our starting point the planetary geostrophic equations (Robinson and Stommel, 1959)

$$f\mathbf{k} \times \mathbf{u} = -\nabla\phi + \nu\nabla^2\overline{\mathbf{u}} + \tau_z, \tag{2.1a}$$

$$0 = -\phi_z + \sigma, \tag{2.1b}$$

$$\nabla_3 \cdot \mathbf{u}_3 = 0, \tag{2.1c}$$

$$\frac{\partial\sigma}{\partial t} + \mathbf{u}_3 \cdot \nabla_3\sigma = \kappa\nabla^2\sigma + \kappa_V \frac{\partial^2\sigma}{\partial z^2}. \tag{2.1d}$$

Here, $\mathbf{u} = (u, v)$ is the horizontal velocity, $\mathbf{u}_3$ is the full velocity, $\overline{\mathbf{u}}$ is the vertically-averaged horizontal velocity, σ is the buoyancy, ϕ the pressure, and τ the Reynolds stress due to wind forcing. ∇ represents the two-dimensional horizontal gradient, and ∇_3 represents the three-dimensional gradient. The boundary conditions are conditions of no normal flow, no stress and no heat flux. There is a rigid lid at $z = 0$, and at the bottom, $z = -H(x, y)$, the velocity satisfies $w = -\mathbf{u} \cdot \nabla H$.

The planetary geostrophic equations, with a rigid lid, are appropriate for dynamics on scales larger than the internal deformation radius, and so they are appropriate for flow in the deep ocean. Their applicability to flow on the continental slope is perhaps questionable, because here the width of the continental slope is not significantly greater than the internal deformation radius. Therefore, although it may not be possible to use these equations to make quantitative predictions of flow on the scale of the slope, they may nonetheless indicate qualitatively the flow patterns that one might expect. Moreover, solutions of these equations provide a starting point to understand solutions of systems of equations with inertia retained. As we shall see, solutions of (2.1) predict phenomena that have previously

been attributed to the presence of inertia; this makes it even more important to understand the noninertial theory before proceeding to more complex models.

In our choice of friction in (2.1a), we have chosen to preserve the thermal wind relation without approximation, which we do by applying the frictional terms in (2.1a) to only the depth-averaged flow. The same form of friction was used in diagnostic calculations by Myers *et al.* (1996). Friction cannot be dispensed with altogether in (2.1a) since not even boundary conditions of no normal flow can be satisfied without some form of friction. We employ lateral downgradient diffusion of vertically-averaged momentum in (2.1a) primarily because of its simplicity. The result is that boundary layers controlled by ν will form in this model where eddies might form in a model with inertia, and this must be kept in mind when interpreting the results of this study.

We now introduce a transport streamfunction ψ, defined by

$$\mathbf{k} \times \nabla\psi = \int_{-H(x,y)}^{0} \mathbf{u}\, dz\,, \tag{2.2}$$

and a wind-stress curl W defined by

$$W = \mathbf{k} \cdot \nabla \times \left(\frac{\tau_s}{H}\right), \tag{2.3}$$

where τ_s is the surface Reynolds stress.

By taking the curl of the vertical average of the momentum equation (2.1a), we can derive the streamfunction equation

$$J\left(\psi, \frac{f}{H}\right) + J\left(\frac{1}{H}, \gamma\right) = W + \nabla^2\nabla \cdot \left(\frac{\nu}{H}\nabla\psi\right), \tag{2.4}$$

where

$$\gamma = -\int_{-H(x,y)}^{0} z\sigma\, dz \tag{2.5}$$

is the vertically-integrated potential-energy density, and the Jacobian

$$J(a, b) \equiv \frac{\partial a}{\partial x}\frac{\partial b}{\partial y} - \frac{\partial a}{\partial y}\frac{\partial b}{\partial x}\,. \tag{2.6}$$

The second Jacobian on the left side of (2.4) vanishes if the ocean is homogeneous, since then we have $\sigma = 0$ (and so $\gamma = 0$). The first Jacobian on the left side of (2.4) then represents the southward distortion of gyres on a western continental slope, as mid-ocean values of ψ follow contours of f/H toward the southwestern corner of the domain, as described by Holland (1967).

The second Jacobian on the left side of (2.4) also vanishes if H is flat, and so this term is

nonzero only when baroclinicity and topography are both present. For this reason it was called the Joint Effect of Baroclinicity And Relief, or JEBAR, by Sarkisyan and Ivanov (1971). Within this framework, (2.4) is to be regarded as a forced advection-diffusion equation for ψ, in which forcing is provided by the wind via W and by the JEBAR term. In the particular case of $\sigma = T(x, y, t)$, γ takes the simple form

$$\gamma = \tfrac{1}{2}H^2T. \tag{2.7}$$

Moreover, since T is independent of z, it is simply advected by ψ. However, if T is independent of z right down to the ocean floor at $z = -H(x, y)$, then there will be heat flux though the floor. We therefore assume that there is a thin bottom boundary layer, at the base of which $\partial T/\partial n = 0$. The effect of this boundary layer on γ can be neglected provided $\kappa_V \ll \kappa$, and our model equations are

$$J\left(\psi, \frac{f}{H}\right) + \frac{1}{2}J(T, H) = W + \nu\nabla^2\zeta, \tag{2.8a}$$

$$H\frac{\partial T}{\partial t} + J(\psi, T) = \nabla \cdot (\kappa H \nabla T), \tag{2.8b}$$

$$\zeta = \nabla \cdot \left(\frac{1}{H}\nabla\psi\right). \tag{2.8c}$$

While interpretations of the dynamics in terms of JEBAR are not always instructive (Cane *et al.,* 1998), the simplicity of (2.8) suggests that it is appropriate to interpret (2.8) using JEBAR.

Owing to the special thermal structure, there are perhaps few physical situations to which the equations (2.8) can be directly applied. However, they are the simplest set of equations in which the interaction between topography and baroclinicity is nontrivial. In this paper, we use these equations to investigate flow over a continental slope. Although we cannot study the influence of the details of the stratification on the flow, we can consider the model problem in which two water masses—one hot, the other cold—are advected onto the continental slope by flow in a hot anticyclonic subtropical gyre and a cold cyclonic subpolar gyre. As the two water masses collide, a strongly baroclinic region must be established. Understanding the nature of this baroclinic region, and placing it within the context of the global solution of these equations, is the primary motivation for the present work. Moreover, any solution obtained using these equations is a solution of (2.1). Similar equations have been proposed by Olbers and Wübber (1991) for flow in a limit in which advection of buoyancy is dominated by the barotropic flow.

We consider an ocean with a flat interior and a smooth western slope on an equatorial β-plane. Co-ordinates are defined such that x increases eastward, and y increases north-

ward. The extreme southwest corner of the domain is the origin of the co-ordinate system. Where appropriate, we shall also use polar co-ordinates (r, θ), where $x = r\cos\theta$ and $y = r\sin\theta$ as usual. We consider topography $H(x, y) = (2H_0/\pi)\tan^{-1}(\lambda x)$, where λ is a constant, so $H = 0$ at $x = 0$ (the western coastline) and $H \to H_0$ (constant) as $x \to \infty$, which we refer to as the "deep ocean."

In the deep ocean, ψ builds up due to wind stress, without interaction with T, since H is assumed to be constant in the deep ocean, and so the JEBAR term vanishes there. Thus, as $x \to \infty$ we have $\psi \to \Psi(y)$, where the function $\Psi(y)$ can be determined in principle from $W(x, y)$. We shall suppose, for simplicity, that the wind stress curl W generates a "double-gyre" streamfunction $\Psi(y)$, with $\Psi(y) = 0$ at $y = 0$ (the equator), $y = 2L$ (the northern boundary), and $y = y_0$ for some $0 < y_0 < 2L$. The latitude $y = y_0$ thus corresponds to the intergyre boundary in the deep ocean. We shall further suppose that $\Psi(y) > 0$ for $0 < y < y_0$, and $\Psi(y) < 0$ for $y_0 < y < 2L$; this corresponds to the typical case of an anticyclonic subtropical gyre and a cyclonic subpolar gyre.

With such a $\Psi(y)$, fluid is advected onto the slope at the extreme northern and southern latitudes, with advection off-slope in mid-latitudes. Therefore, we must specify the temperature T offshore in the northern part of the subpolar gyre and the southern part of the subtropical gyre, where the temperature is advected onshore by the flow. For simplicity, we shall assume that the temperature takes a single, different, uniform value in each of these two regions, with a difference of magnitude $\mathscr{T}$. For definiteness, we shall suppose that $T = 0$ in the equatorial region, and $T = -\mathscr{T}$ in the polar region. The model problem to be considered, therefore, consists in understanding the interaction of two fluids of different, uniform temperature, brought together on a continental slope by the action of two barotropic gyres of opposite circulation. It seems reasonable to suppose that the present model captures some of the essential dynamics of this problem, especially if, as we might reasonably suppose, the baroclinic current that separates subtropical and subpolar gyres arises from primarily *horizontal* advection of water masses of substantially different temperature. In mid-latitude regions where advection is offslope, the value of the temperature offshore is not specified but, rather, determined by the dynamics on the slope. In this paper we do not discuss the dynamics of the deep ocean, but we shall assume that thermal forcing over the deep ocean is always strong enough to return the temperature to one of the two values 0 or $-\mathscr{T}$ by the time the fluid has been advected round the subtropical or subpolar gyre, respectively.

The problem is now nondimensionalized as follows. For our length scale we use L, which is the meridional length scale of a gyre. For our velocity scale U, we use the velocity associated with the streamfunction ψ, so that $\psi_{\max} = UHL$ defines U. A time scale is readily derived from L and U, but it is not required here, since we consider only steady flow. The scale T_s for the temperature is derived from (2.8a): $HT_s/L^2 = \beta\psi/LH = \beta U$; i.e. $T_s = L^2\beta U/H$. The small parameters ν and κ are nondimensionalized using LU.

In this paper we shall seek steady-state solutions consistent with boundary conditions in

the deep ocean which we have assumed to be independent of time. The problem is thus stated in nondimensional variables as follows:

$$J\left(\psi, \frac{y}{H}\right) + \frac{1}{2} J(T, H) = W + \nu \nabla^2 \zeta, \tag{2.9a}$$

$$J(\psi, T) = \nabla \cdot (\kappa H \nabla T), \tag{2.9b}$$

$$\zeta = \nabla \cdot \left(\frac{1}{H} \nabla \psi\right). \tag{2.9c}$$

where

$$H(x, y) = \frac{2}{\pi} \tan^{-1}(\lambda x), \tag{2.10}$$

and boundary conditions are

$$\psi = 0 \quad \text{on} \quad y = 0, \quad y = 2 \quad \text{and} \quad x = 0, \tag{2.11a}$$

$$\zeta = 0 \quad \text{on} \quad y = 0, \quad y = 2 \quad \text{and} \quad x = 0, \tag{2.11b}$$

$$\psi \to \Psi(y) \quad \text{as} \quad x \to \infty, \tag{2.11c}$$

$$T_n = 0 \quad \text{on} \quad y = 0, \quad y = 2 \quad \text{and} \quad x = 0, \tag{2.11d}$$

$$T \to 0 \quad \text{if} \quad \Psi'(y) > 0, \quad y < y_0 \quad \text{as} \quad x \to \infty, \tag{2.11e}$$

$$T \to -\mathscr{T} \quad \text{if} \quad \Psi'(y) > 0, \quad y > y_0 \quad \text{as} \quad x \to \infty, \tag{2.11f}$$

$$T_n \to 0 \quad \text{if} \quad \Psi'(y) < 0 \quad \text{as} \quad x \to \infty. \tag{2.11g}$$

The situation is depicted in Figure 1.

The condition (2.11a) corresponds to no normal flow at the boundaries. The boundary condition (2.11b) corresponds to a free slip boundary condition. A condition of either no slip or free slip is required by the form of friction we have chosen in (2.1a). We have chosen free slip for convenience. In fact, only one result presented in the subsequent sections depends on this choice of boundary condition. The boundary condition (2.11c) specifies the streamfunction that is built up by wind forcing in the deep ocean. The condition (2.11d) states that there is no flux of heat through the boundaries. Boundary conditions (2.11e) and (2.11f) specify the temperature of the water being advected onto the shelf by the subtropical and subpolar gyres, respectively. The boundary condition (2.11g) states simply that there is no boundary layer in T as $x \to \infty$, so the value of T in the limit $x \to \infty$ when $\Psi'(y) < 0$ is determined by dynamics on the shelf, and the value of T is then advected off-shelf by ψ. Note that we require $\Psi(y) = 0$ for $y = 0$, $y = 2$ and $y = y_0$ for some y_0 that satisfies $0 < y_0 < 2$. The precise form of $\Psi(y)$ is not required for Sections 3 and 4. All that

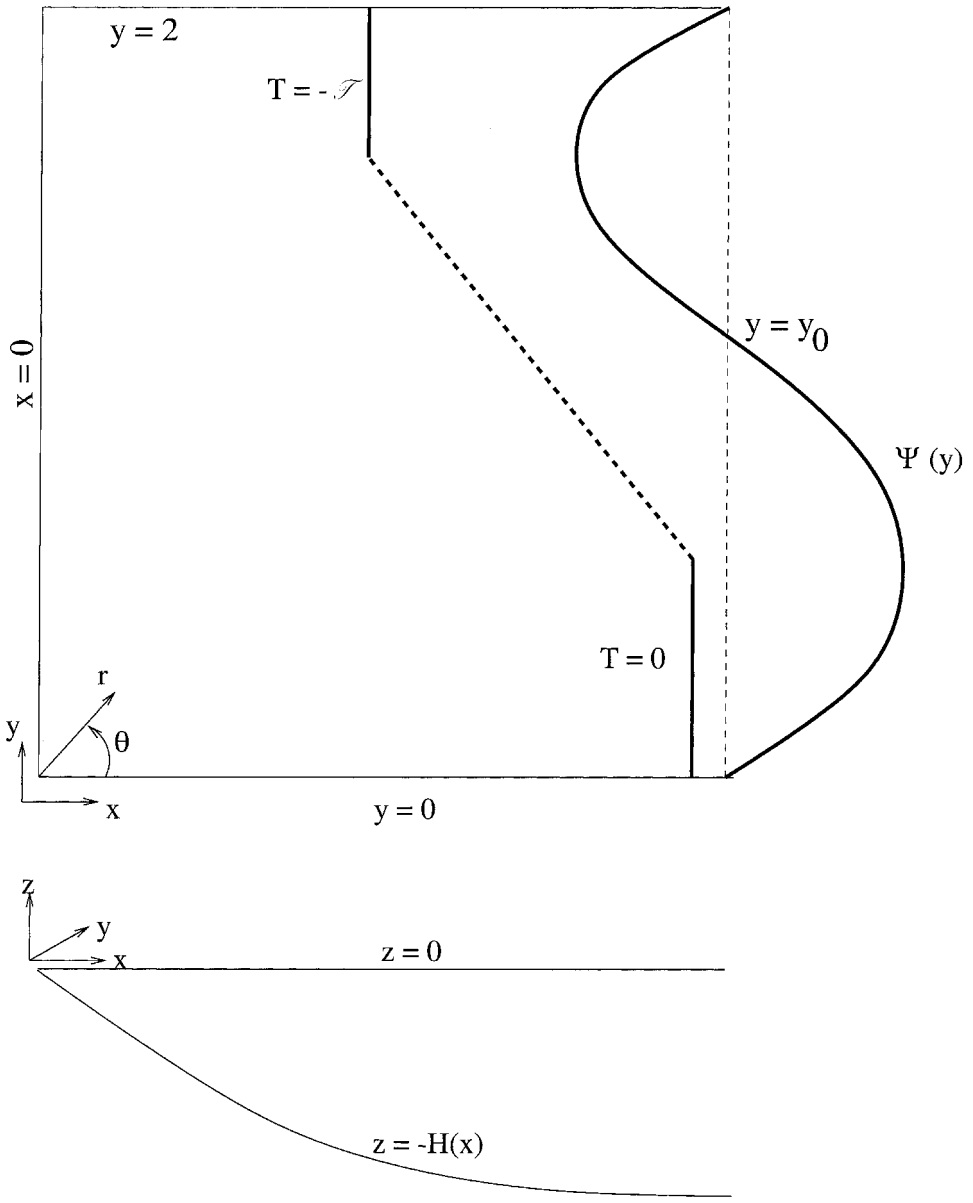

Figure 1. A schematic picture showing (upper figure) a plan view of the domain of interest, with deep-ocean streamfunction $\Psi(y)$ and temperature $T(y)$ indicated; and (lower figure) the profile of the bathymetry.

is required in these sections is the value of $|\Psi'(y_0)|$. We shall discuss the form of $\Psi(y)$ further in Section 5. Henceforth, we consider the limit in which both $\nu \ll 1$ and $\kappa \ll 1$, with $\nu/\kappa = O(1)$.

3. Solution for small $\mathscr{T}$

To develop understanding of these equations, we consider first the limit of small $\mathscr{T}$. We shall assume in this section that $\mathscr{T}$ is sufficiently small that the JEBAR term is negligible to leading order. That is, we expand

$$\psi = \psi_0 + \mathscr{T}\psi_1 + O(\mathscr{T}^2), \tag{3.1a}$$

$$T = \mathscr{T}T_1 + O(\mathscr{T}^2). \tag{3.1b}$$

In this section, $\mathscr{T}$ and ν are independent, small parameters. Therefore, ψ and T must be represented as double expansions in $\mathscr{T}$ and ν. This means that each of the terms ψ_0 and ψ_1 in (3.1a), and T_1 in (3.1b) represents a perturbation expansion in ν, and each expansion starts at an order that must be determined as part of the solution procedure. In this section we determine the order at which each expansion starts, and the leading term in each expansion. Higher orders in ν, for each order in $\mathscr{T}$, are not required.

In Section 3a we obtain the leading-order streamfunction ψ_0. In Section 3b we obtain the leading-order temperature T_1, and in Section 3c we determine the "perturbation streamfunction" ψ_1. Throughout this section and the next, we shall use the term "perturbation streamfunction" to refer to the total streamfunction minus the streamfunction in the barotropic limit $\mathscr{T} = 0$.

a. The streamfunction to O(1)

On substitution of (3.1) into (2.9a), we have, at leading order,

$$J\left(\psi_0, \frac{y}{H}\right) = \nabla^2\nabla \cdot \left(\frac{\nu}{H}\nabla\psi_0\right). \tag{3.2}$$

Eq. (3.2) must now be solved in the limit $\nu \to 0$. Two asymptotic regions are required: $r = O(1)$ and $r = O(\nu^{1/3})$.

In the region $r = O(1)$, ψ_0 satisfies

$$J\left(\psi_0, \frac{y}{H}\right) = 0. \tag{3.3}$$

Eq. (3.3) states that ψ_0 is a function of y/H over the slope, which is set by the conditions in the deep ocean. The solution is

$$\psi_0 = \Psi\left(\frac{y}{H}\right). \tag{3.4}$$

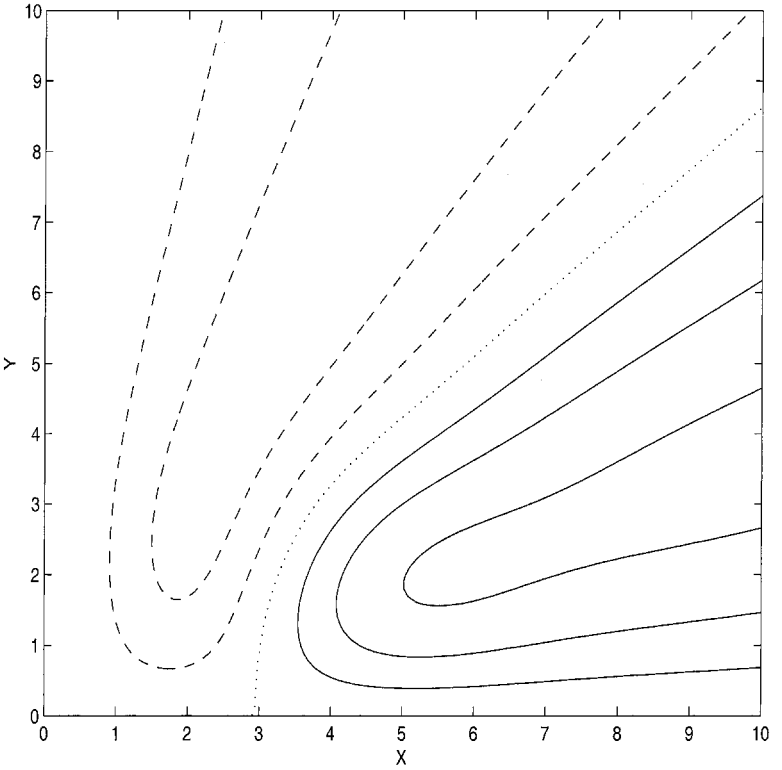

Figure 2. A typical numerical solution depicting the structure of ψ_0 in the region $r = O(\nu^{1/3})$. Contours of $\psi > 0$ are shown in solid lines, and those of $\psi < 0$ are shown in dashed lines. The contour $\psi = 0$ is the dotted line. The co-ordinates X and Y are the co-ordinates of the corner region. For details, see Appendix A.

This solution is valid everywhere except in the limit $r \to 0$, where y/H contours converge, and so infinite gradients of ψ are formed. Thus a second region is required, in which diffusion is important. We define a re-scaled co-ordinate R appropriate to this corner region, such that $R = \nu^{-1/3} r$. For later use, we also define re-scaled co-ordinates X and Y such that $X = \nu^{-1/3} x$ and $Y = \nu^{-1/3} y$. Then, in the region $R = O(1)$, (3.2) is

$$\frac{\partial \psi_0}{\partial R} = \cos^2\theta \left(\frac{\partial^2}{\partial R^2} + \frac{1}{R}\frac{\partial}{\partial R} + \frac{1}{R^2}\frac{\partial^2}{\partial \theta^2} \right) \left[\frac{1}{\cos\theta} \left(\frac{\partial^2}{\partial R^2} + \frac{\cos\theta}{R^2}\frac{\partial}{\partial \theta} \left(\frac{1}{\cos\theta}\frac{\partial}{\partial \theta} \right) \right) \psi_0 \right]. \quad (3.5)$$

This equation must be solved subject to boundary conditions $\psi_0 \to \Psi[(\pi/2\lambda)\tan\theta]$ as $R \to \infty$, and free-slip boundary conditions on $\theta = 0, \pi/2$.

A typical numerical solution of (3.5) is shown in Figure 2. Details of this solution, and of the numerical method used to obtain it, are given in Appendix A. This is the only result presented in this paper which depends upon the choice of free-slip versus no-slip boundary condition. In the absence of viscosity, the contours of ψ_0 would be straight lines, meeting at

the southwest corner of the domain $(x, y) = (0, 0)$. In Figure 2 we see that the effect of diffusion is to remove that singularity. Instead, the subpolar gyre ($\psi < 0$) and subtropical gyre ($\psi > 0$) meet along the line ($\psi = 0$) that extends from a stagnation point on the southern boundary through the corner region. As $R \to \infty$ this line follows the contour $y/H = y_0$.

In this paper, our interest is the effect of temperature on the streamfunction and in Section 3c we compute this correction. The calculation requires the temperature, T_1, which can be computed from ψ_0. This we do in Section 3b. In all these calculations, we bear in mind that, in principle, corrections at higher-order in ν will exist, but the leading-order description is sufficient here.

b. The temperature to $O(\mathscr{T})$

The equation for T_1 is obtained by substitution of (3.1) into (2.9b). The result is

$$J(\psi_0, T_1) = \nabla \cdot (\kappa H \nabla T_1). \tag{3.6}$$

In the limit $\kappa \to 0$, this equation is simply

$$J(\psi_0, T_1) = 0, \tag{3.7}$$

and this has the solution

$$T_1 = T_1(\psi_0). \tag{3.8}$$

The temperature is set in the deep ocean and advected onto the slope. In the southern part of the subtropical gyre, where advection by ψ is on-slope, the temperature takes the value $T = 0$. Likewise, in the northern part of the subpolar gyre, where advection by ψ is also on-slope, the temperature takes the value $T = -\mathscr{T}$. The solution to (3.8) consistent with these deep-ocean conditions is

$$T_1 = \begin{cases} -1 & \text{if} \quad \psi_0(x, y) < 0 \\ 0 & \text{if} \quad \psi_0(x, y) > 0 \end{cases}. \tag{3.9}$$

The solution (3.9) simply states that, if thermal diffusion is neglected, temperature is constant on streamlines. This applies in both $r = O(1)$ and $r = O(\nu^{1/3})$. However, it leads to discontinuous temperature where $\psi = 0$ away from boundaries, and so a thermal boundary layer will form in the neighborhood of $\psi = 0$.

The boundary layer forms because hot and cold fluid from the two gyres initially meet at the stagnation point $(X, Y) = (X_0, 0)$, say, where the dashed contour $\psi = 0$ in Figure 2 meets the southern boundary (for the case presented in Fig. 2, $X_0 \approx 3$). Here, ψ_0 takes the form $\psi_0 = DY(X - X_0)$, where $D > 0$ is a constant, and a region forms about this stagnation point in which thermal diffusion acts to remove the discontinuity in T. By considering a balance of terms in (3.6), we can see that the scale of this region, in which the thermal diffusion must be significant in both X and Y directions, is given by $(X - X_0, Y) = O(\kappa^{1/2}, \nu^{1/6}, \kappa^{1/2}, \nu^{1/6})$.

Fluid from this stagnation point region is then ejected through the corner region $r = O(\nu^{1/3})$ within a thin internal thermal boundary layer. In this boundary layer there is a balance between advection and thermal diffusion, in which the latter must be significant in the direction across the layer. Thus, the layer is centered on the contour $\psi = 0$, and has a thickness which is $O(\kappa^{1/2}\nu^{1/6})$ relative to the scale of the corner region. Since the corner region is itself of scale $O(\nu^{1/3})$ relative to the scale of the gyres and the shelf, the thickness of the internal boundary layer in the corner region relative to the imposed length scales of the problem is $O(\kappa^{1/2}\nu^{1/2})$.

In the region $r = O(1)$, Eq. (3.6) still holds for T_1, and the thermal boundary layer that forms in the corner region is ejected onto the main shelf. A balance of terms in (3.6) implies that, over the main shelf, the thermal boundary layer has thickness $O(\kappa^{1/2})$, centered on the contour $\psi = 0$ (or, equivalently, centered on $y/H = y_0$). It thus extends from the corner region across the slope to the intergyre boundary. Since the thermal boundary layer has a narrow horizontal scale, and separates regions of hot and cold fluid, we shall refer to it as a "front."

The width of the front over the slope is $O(\kappa^{1/2})$, which is greater than its width in the corner region, which is $O(\kappa^{1/2}\nu^{1/2})$. This is to be expected, because advection is very strong in the corner region, since the entire transport of both gyres passes through this region of horizontal scale $O(\nu^{1/3})$ and of depth $O(\nu^{1/3})$, and so any balance between advection and thermal diffusion must be expected to lead to relatively thin thermal boundary layers in such a region. Lengthy but straightforward analysis shows that the solution for T_1 can be written in both regions in terms of error functions, and that the front in the corner region $R = O(1)$ thickens in the limit $R \to \infty$, in a manner consistent with the scale that it must have over the main continental slope $r = O(1)$.

This completes the description of T_1. In the present, linear theory we have assumed that $\mathscr{T}$ is sufficiently small that the front does not affect the leading-order streamfunction ψ_0. The first correction to ψ due to the front is computed in Section 3c.

c. The streamfunction to $O(\mathscr{T})$

We now compute the first-order (in $\mathscr{T}$) correction to ψ induced by the $O(\mathscr{T})$ term $J(T, H)$ in (2.9a). Although our interest subsequently will be in much larger values of $\mathscr{T}$, the analysis for small $\mathscr{T}$ is instructive, and we take the opportunity in this section to establish notation that will subsequently be used in Sections 4 and 5.

We consider first the region $r = O(1)$; that is, the region over the slope away from the equatorial corner. The perturbation streamfunction ψ_1 satisfies

$$J\left(\psi_1, \frac{y}{H}\right) + \frac{1}{2} J(T_1, H) = \frac{\nu}{H} \frac{\partial^4 \psi_1}{\partial n^4}, \tag{3.10}$$

where n is a co-ordinate that measures distance normal to the contour $y/H = y_0$. Eq. (3.10) is not a formal asymptotic equation for ψ_1, but the diffusion operator on the right side of (3.10) has been approximated on the assumption that it is significant only in a narrow

region centered on the front, so that the normal derivatives dominate, and their effect on H is negligible. Note, however, that the first Jacobian in (3.10) cannot be approximated in the same way, because the front follows a contour of constant y/H, and so $J(\psi_1, y/H) = (\partial\psi_1/\partial s)(d(y/H)/dn)$, where s is a co-ordinate that measures distance along the contour $\psi = 0$ from the equatorial corner.

In seeking solutions of Eq. (3.10), a balance between the advection of ψ_1 by y/H and the diffusion is required, and this in turn requires a viscous boundary layer of thickness $O(\nu^{1/4})$. This viscous boundary layer is, therefore, much thicker than the thermal boundary layer, or front, of thickness $O(\kappa^{1/2})$, across which T varies from $-\mathscr{T}$ to 0. Therefore, we shall obtain an equation for ψ_1 in a region in which $n = O(\nu^{1/4})$, and replace $\partial T_1/\partial n$ by $-\delta(n)$, where $\delta(n)$ denotes the usual Dirac delta function.

In fact, it is convenient to use stretched tangential and normal co-ordinates, as follows. In place of the normal co-ordinate n we shall use ξ defined by

$$\xi = \beta(s)n, \tag{3.11}$$

where

$$\beta(s) = |\nabla(y/H)|. \tag{3.12}$$

Here $\beta(s)$ represents the strength of the combined planetary and topographic β effect, and so the normal co-ordinate ξ varies most rapidly in space when β is strongest. In the barotropic limit, the contours of ψ are straight, parallel lines when ξ is used as normal co-ordinate, and any departure of ψ from straight parallel lines is an effect of baroclinicity.

Eq. (3.10) is now expressed in terms of the normal co-ordinate ξ and *any* along-contour co-ordinate $\chi = \chi(s)$ as:

$$\frac{\partial\psi_1}{\partial\chi} + \frac{1}{2}\frac{dH}{d\chi}\delta(\xi) = \nu[J(\chi, \xi)]^{-1}\frac{\beta^4(\chi)}{H(\chi)}\frac{\partial^4\psi_1}{\partial\xi^4}. \tag{3.13}$$

where $J(\chi, \xi)$ is the Jacobian of the co-ordinate transformation.

We now define an appropriate boundary-layer co-ordinate $\xi' = \nu^{-1/4}\xi$, so ξ' has order-one variations when ξ is on the boundary-layer scale $\xi = O(\nu^{1/4})$. We also rescale the streamfunction ψ_1, writing $\psi_1 = \nu^{-1/4}\psi'_1$, implying that ψ_1 has a magnitude $O(\nu^{-1/4})$. We now drop the primes on ψ_1 and ξ, and the equation for ψ_1 is thus

$$\frac{\partial\psi_1}{\partial\chi} + \frac{1}{2}\frac{dH}{d\chi}\delta(\xi) = [J(\chi, \xi)]^{-1}\frac{\beta^4(\chi)}{H(\chi)}\frac{\partial^4\psi_1}{\partial\xi^4}. \tag{3.14}$$

The co-ordinate $\chi(s)$ is a general along front co-ordinate. The form of the right-hand side of (3.14) suggests the use of a particular choice for $\chi(s)$, namely $\rho(s)$, defined such that

$$J(\rho, \xi) = \frac{\beta^4(\rho)}{H(\rho)}. \tag{3.15}$$

We note that $\rho \propto x$ as $x \to \infty$ and $-\rho \propto r^{-3}$ as $r \to 0$. Thus the deep ocean $x \to \infty$ corresponds to the limit $\rho \to \infty$, and the equatorial corner $r = 0$ corresponds to the limit $\rho \to -\infty$. The location of the origin of the co-ordinate $\rho = 0$ is arbitrary. Using the co-ordinate ρ, (3.14) is

$$\frac{\partial \psi_1}{\partial \rho} + \frac{1}{2}\frac{dH}{d\rho}\,\delta(\xi) = \frac{\partial^4 \psi_1}{\partial \xi^4}\,. \tag{3.16}$$

Subsequently, the analysis will take advantage of the mathematical simplification afforded by use of the co-ordinate ρ but, wherever possible, results will be presented relative to physical co-ordinates.

Eq. (3.16) is solved by Fourier transformation in ξ, integration with respect to ρ', and then inversion of the Fourier transform. We impose the boundary condition $\psi_1 \to 0$ as $\rho \to \infty$, because the perturbation streamfunction must be zero in the deep ocean. The result is

$$\psi_1 = \frac{1}{4\pi}\int_{-\infty}^{\infty} dk \int_{\rho}^{\infty} \frac{dH(\rho')}{d\rho'} \exp\{ik\xi - k^4(\rho' - \rho)\}\, d\rho'. \tag{3.17}$$

Eq. (3.17) is evaluated numerically, using a second-order accurate method to evaluate the integral with respect to ρ, for each k, followed by a Fast Fourier Transform for the integral with respect to k. The solution depends in detail on the shape of the topography, and with topography of form $H(x) = (2/\pi)\tan^{-1}(\lambda x)$ it is not possible to scale out the parameter λ. Therefore, in Figure 3 we show the contours of y/H, and in Figure 4 we present solutions for ψ_1 for $\lambda = 0.1, 1.0, 10.0$ with $y/H = 1.0$, and in Figure 5 for $y/H = 0.5$, 1.0, 1.5 with $\lambda = 1.0$.

In all cases, we see that the JEBAR term induces an anticyclonic secondary circulation on the slope. This is as expected: the topography is an increasing function of x, so $J(T, H) > 0$ because the northern waters are colder than the southern waters. From (2.8a) this means that we expect ψ to increase as we travel along a contour of y/H from the deep ocean to the equatorial corner, where viscosity then becomes important. Despite the wide range of values of λ considered, there is little qualitative difference between cases presented here. In each case, an anticyclonic secondary circulation is induced, centered on the front over the sloping topography. This means that streamlines will tend to be deflected to the north of their location in the barotropic theory.

The solution for ψ_1 given by (3.17) is evaluated without consideration of the dynamics of the equatorial corner region $r = O(\nu^{1/3})$. Moreover, it appears from the solutions presented in Figures 4 and 5 that $\psi_1 \to 0$ as $x \to 0$, and so no modification to ψ is required in the corner region $r = O(\nu^{1/3})$. To check this, we examine the solution (3.17) in the limit $\rho \to -\infty$.

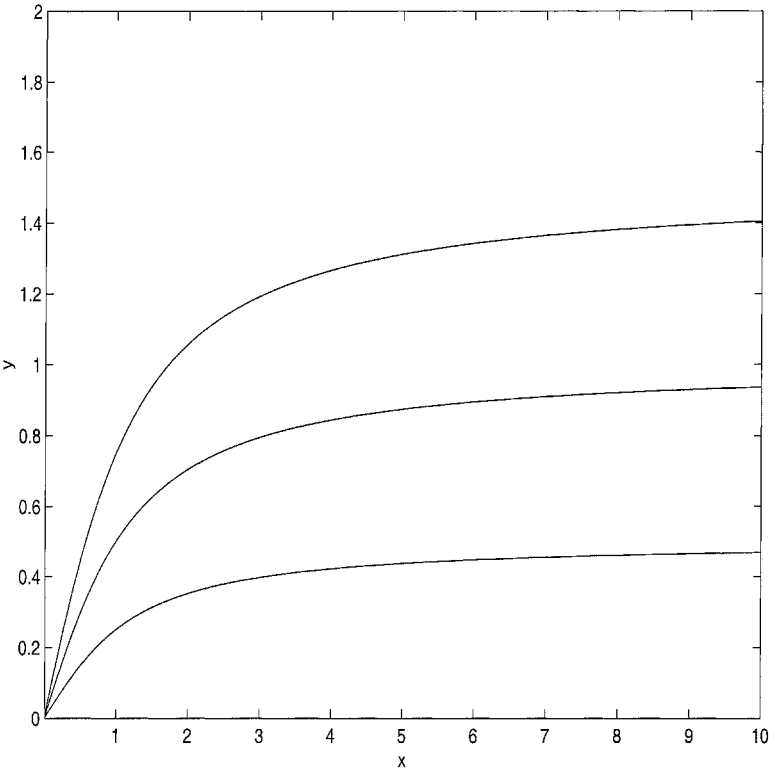

Figure 3. Contours of $y/H = 1.5$ (top line), 1.0 (middle line), and 0.5 (bottom line), for $H(x) = (2/\pi)\tan^{-1}\lambda x$. The case $\lambda = 1$ is shown; other values of λ correspond simply to a re-scaling of the x co-ordinate and are therefore not shown.

The dominant contribution in the integral with respect to ρ' in (3.17) comes from the region $\rho' = O(1)$, and for large negative ρ (3.17) is approximately

$$\psi_1 = \frac{1}{4\pi}\int_{-\infty}^{\infty} dk \int_{-\infty}^{\infty} \frac{dH(\rho')}{d\rho'} \exp\{ik\xi + k^4\rho\}\, d\rho' \\ = (-\rho)^{-1/4}\frac{1}{4\pi}\int_{-\infty}^{\infty} \exp\left\{ik\left[\frac{\xi}{(-\rho)^{1/4}}\right] - k^4\right\} dk. \tag{3.18}$$

Eq. (3.18) shows that ψ_1 should indeed vanish as $r \to 0$, which corresponds to the limit $\rho \to -\infty$. In the limit $\rho \to -\infty$, ψ_1 is a function of $\xi/(-\rho)^{1/4}$ multiplied by $|\rho|^{-1/4}$, and the function of $\xi/(-\rho)^{1/4}$ is simply the inverse Fourier transform of $\frac{1}{2}e^{-k^4}$. This may be expressed in terms of generalized hypergeometric functions (Slater, 1966).

Now, the solutions presented in this section for ψ_1 were obtained on the assumption that the perturbation streamfunction given by (3.17) is small compared with the leading-order streamfunction. Recall that the streamfunction ψ_1 was re-scaled on $\nu^{-1/4}$, while the leading-order streamfunction ψ_0 will be $O(\nu^{1/4})$ in the region $(y/H - y_0) = O(\nu^{1/4})$. It

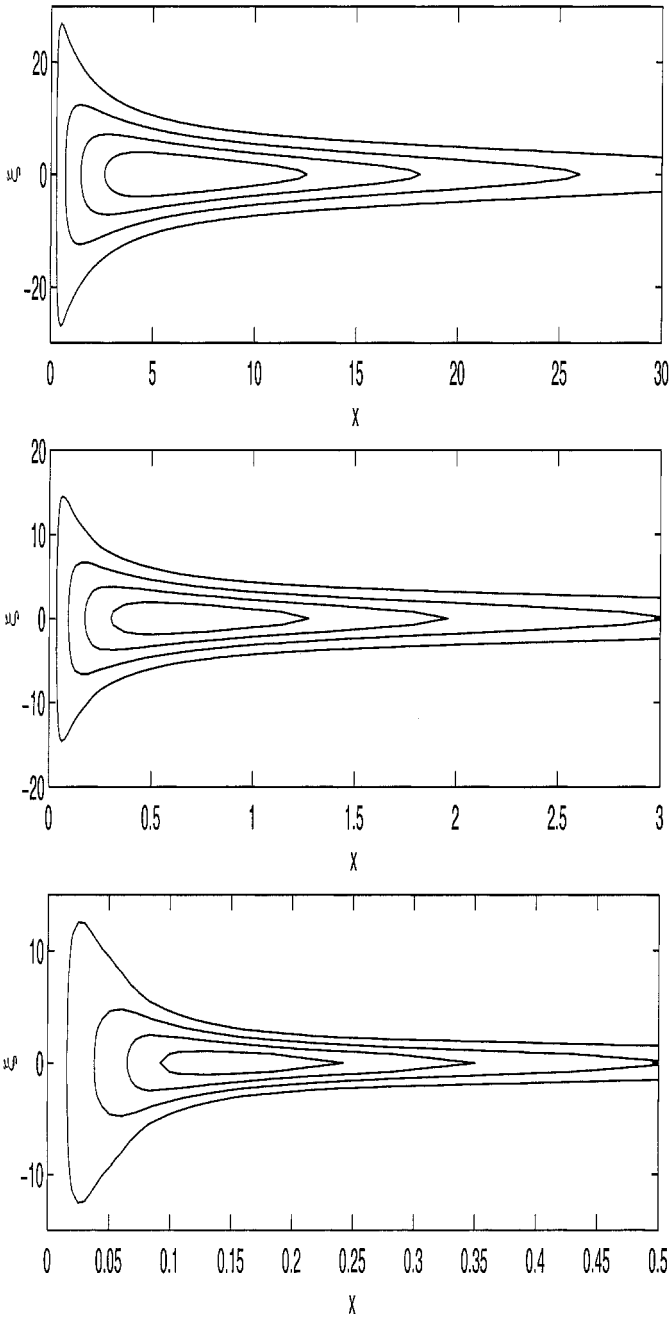

Figure 4. Linear perturbation streamfunction for $y/H = 1$ and $\lambda = 0.1$ (top panel), $\lambda = 1.0$ (middle panel) and $\lambda = 10$ (bottom panel). The contour levels are $\{0.01, 0.02, 0.03, 0.04\}$ (top panel) and $\{0.02, 0.04, 0.06, 0.08\}$ (other panels). Note well the co-ordinates used: the left-right co-ordinate is x, the distance from the coast, and the top-bottom co-ordinate used is the boundary-layer co-ordinate ξ. The entire left axis of each figure thus corresponds to the single point $r = 0$. The x-scales in the three figures are different because the width of the slope decreases as λ increases (top to bottom).

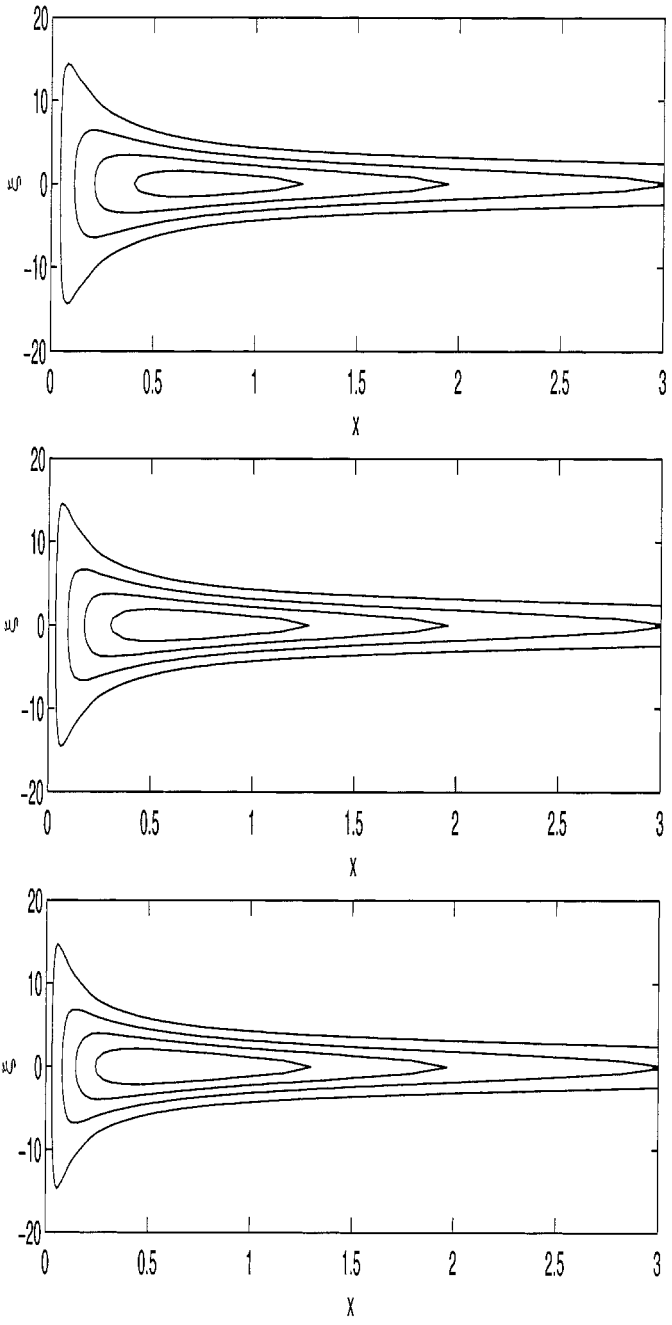

Figure 5. Linear perturbation streamfunction for $\lambda = 1.0$ and $y/H = 1.5$ (top panel), $y/H = 1.0$ (middle panel) and $y/H = 0.5$ (bottom panel). The contour levels are {0.02, 0.04, 0.06, 0.08} in all panels. The middle panel of this figure is identical to the middle panel of Figure 4, and is repeated here for reference. Details of co-ordinates used are as in Figure 4.

follows that the perturbation expansion must break down when $\mathscr{T}\nu^{-1/4} = O(\nu^{1/4})$, i.e. $\mathscr{T} = O(\nu^{1/2})$. On this scale, the perturbation streamfunction is sufficiently strong to move the contour $\psi = 0$ by a distance $O(\nu^{1/4})$, and so the front will no longer lie on $\xi = 0$.

The conclusions to be drawn from the analysis of this section are that a solution can be constructed to this problem, at least for small $\mathscr{T}$. We have seen that, as $\mathscr{T}$ is increased, the asymptotic structure breaks down first in the region $r = O(1)$, $(y/H - y_0) = O(\nu^{1/4})$, because the perturbation streamfunction induced by JEBAR becomes of the same order (i.e. $O(\nu^{1/4})$) as the leading-order streamfunction in that region. Furthermore, the front, which follows $\psi = 0$, departs from $\xi = 0$ by $(\Delta\xi) = O(\mathscr{T}\nu^{-1/2})$, and so when $\mathscr{T} = O(\nu^{1/2})$ the location of this layer is not known *a priori,* on the scale $\xi = O(1)$, but must instead be determined as part of the solution. We analyze this regime in Section 4.

4. The weakly nonlinear regime $\mathscr{T} = O(\nu^{1/2})$

The preceding analysis shows that, as $\mathscr{T}$ is increased, nonlinearity first arises in these equations when $\mathscr{T} = O(\nu^{1/2})$. In this section we show how a nonlinear integral equation can be derived for the location of the front, and solve it to obtain ψ for a wide range of values of $\mathscr{T}/\nu^{1/2}$.

We anticipate the scaling for $\mathscr{T}$ derived in Section 3, and define a re-scaled temperature parameter T, such that

$$\mathsf{T} = \mathscr{T}\nu^{-1/2}. \tag{4.1}$$

Throughout Section 4, T will be of order unity. Also, we are concerned with the region $\xi = O(1)$, in which $\psi = O(\nu^{1/4})$. Therefore, throughout Section 4 we replace ψ with $\nu^{1/4}\psi$.

The location $\xi = \xi_0(\rho)$ corresponds to the location of the front (of thickness $O(\kappa^{1/2})$). As in Section 3, the perturbation streamfunction is of significant magnitude in a region of width $O(\nu^{1/4})$ about the front. This is much broader than the scale of temperature variations within the front, which is of thickness $O(\kappa^{1/2})$. Thus, the temperature takes the form

$$T = \begin{cases} -\mathscr{T} & \text{for} \quad \xi > \xi_0(\rho) \\ 0 & \text{for} \quad \xi < \xi_0(\rho) \end{cases} \tag{4.2}$$

with $\psi = 0$ along $\xi = \xi_0(\rho)$. The solution that we obtain for ψ must be consistent with this temperature distribution: values of $\xi > \xi_0$ must correspond to subpolar waters, with $\psi < 0$, and similarly $\xi < \xi_0$ must correspond to subtropical waters, with $\psi > 0$. We shall see that the solutions obtained are consistent with this, even when a re-circulating gyre is present at the larger values of T investigated.

Using the system of co-ordinates (ρ, ξ) established in the previous section, the equation for ψ in the region $(y/H - y_0) = O(\nu^{1/4})$ is

$$\frac{\partial\psi}{\partial\rho} + \frac{\mathsf{T}}{2}\frac{dH}{d\rho}\delta(\xi - \xi_0(\rho)) = \frac{\partial^4\psi}{\partial\xi^4}. \tag{4.3}$$

Eq. (4.3) corresponds to Eq. (3.16) for ψ_1, except that the location of the front $\xi_0(\rho)$ is not known in advance but must be determined as part of the solution procedure. The additional condition required is that the streamfunction must be zero all along the front, since the front is too thin for diffusion to balance gradients in ψ. The problem thus takes the mathematical form of a Stefan problem, except that the usual second-order diffusion is replaced by fourth-order diffusion, and the Stefan-problem boundary condition relating the value of ψ and its normal derivative at $\xi = \xi_0(\rho)$ is replaced by the much simpler condition $\psi = 0$ at $\xi = \xi_0(\rho)$. The Stefan problem and its solution are discussed in detail in Crank (1984), but in this paper the theory is developed as required.

As in Section 3 for (3.16), we proceed by Fourier transformation in ξ, integration with respect to ρ, and then inversion of the Fourier transform. Again, we impose the boundary condition of no perturbation streamfunction in the deep ocean (boundary condition 2.11c). The result is

$$\psi = -c\xi + \frac{\mathsf{T}}{4\pi}\int_{-\infty}^{\infty} dk \int_{\rho}^{\infty} \frac{dH(\rho')}{d\rho'} \exp\{ik[\xi - \xi_0(\rho')] - k^4(\rho' - \rho)\}\, d\rho'. \qquad (4.4)$$

where the positive constant c is defined by

$$c = -\Psi'(y_0). \qquad (4.5)$$

From (4.4), the condition that $\psi = 0$ at $\xi = \xi_0(\rho)$ implies that the following nonlinear integral equation for $\xi_0(\rho)$ must hold:

$$c\xi_0(\rho) = \frac{\mathsf{T}}{4\pi}\int_{-\infty}^{\infty} dk \int_{\rho}^{\infty} \frac{dH(\rho')}{d\rho'} \exp\{ik[\xi_0(\rho) - \xi_0(\rho')] - k^4(\rho' - \rho)\} d\rho'; \qquad \xi_0 \to 0 \quad \text{as} \quad \rho \to \infty. \qquad (4.6)$$

a. Numerical solutions

We have obtained numerical solutions to (4.6), and hence evaluated (4.4) to obtain the streamfunction ψ for $\mathsf{T}/c = 1, 10, 10^2, 10^3$ and 10^4. Henceforth we take $c = 1$; solutions for other values of c can be obtained from the same value of T/c by multiplying the entire solution (but not $\xi_0(\rho)$) by c. The numerical solution proceeds in two stages. First, the nonlinear integral equation (4.6) must be solved for ξ_0; then, the integral (4.4) must be evaluated for all values of ξ.

It is shown in Appendix B that ξ_0 decays as $x^{-5/4}$ as $x \to \infty$, and so by starting the integration at a sufficiently-large value of ρ, we may start with $\xi_0 = 0$. We then integrate (4.6) in the direction of decreasing ρ, using Newton's method to solve the nonlinear equations that determine $\xi_0(\rho)$. The number of points in k is held fixed at 512, except for the case $\mathsf{T} = 10^4$ shown in Figure 10, where 2048 points were required. The grid spacing (Δk) decreases as $\rho \to -\infty$, with (Δk) proportional to $(-\rho)^{-1/4}$, and the maximum value of k, $k_{\max} = (10/|\rho|)^{1/4}$ as $\rho \to -\infty$.

In Figure 6 we show the streamfunction for $\mathsf{T} = 1.0$. For this value of T there is barely

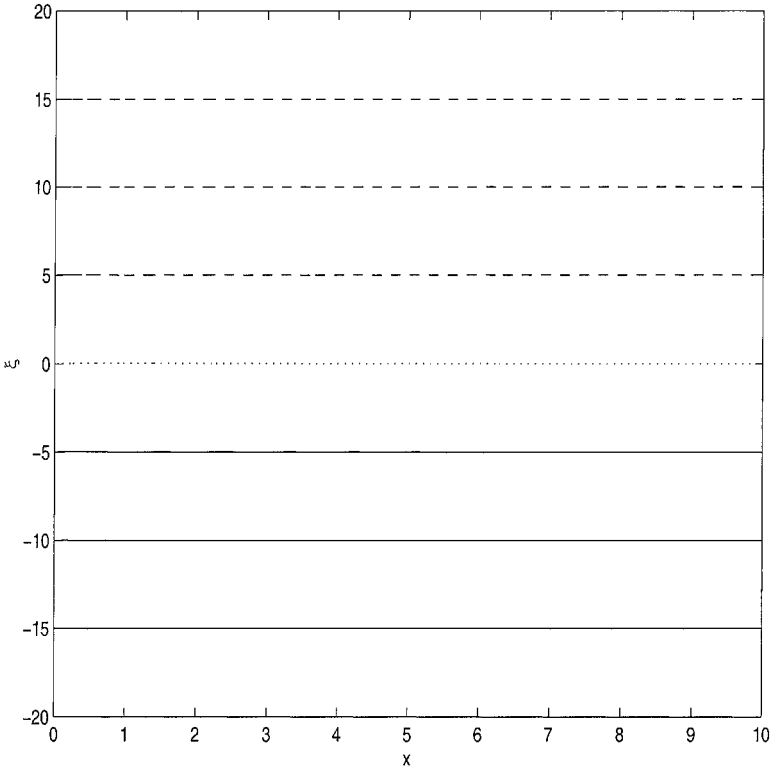

Figure 6. Contours of the streamfunction at $\mathsf{T} = 1.0$. Note that, in common with Figures 4 and 5, we use co-ordinates x and ξ in this figure. In common with Figure 2, we use solid contours for $\psi > 0$, dashed contours for $\psi < 0$, and a dotted contour for $\psi = 0$. Contour levels are equally spaced, with a contour interval of 5.

any noticeable effect on the streamfunction. The perturbation streamfunction (not shown) takes the form of ψ_1 predicted in Section 3.

In Figure 7 we show the streamfunction in the case $\mathsf{T} = 10$. Here we can see that, as we approach $x = 0$, the streamlines are becoming deflected slightly to the north, as predicted in Section 3. Note especially the location of the contour $\psi = 0$ (dashed line), which corresponds to the location of the temperature jump.

As T is increased further, the structure of the solution begins to change. The solution for $\mathsf{T} = 10^2$ is shown in Figure 8. In this figure, the large area between the contour $\psi = 0$ and the first positive contour of ψ suggests that a gyre might form to the south of the contour $\psi = 0$ on the slope ($x \leq 1$). In Figure 9 we see that a gyre does indeed form to the south of the contour $\psi = 0$ on the slope when $\mathsf{T} = 10^3$.

It is interesting to note in Figure 8 that, although the contours are displaced as x decreases, they all appear to return to their initial values of ξ as $x \to 0$. In fact, it is shown in Appendix C that $\psi = -\xi + O(r^{3/4})$ as $r \to 0$. Thus, as the equatorial corner is approached,

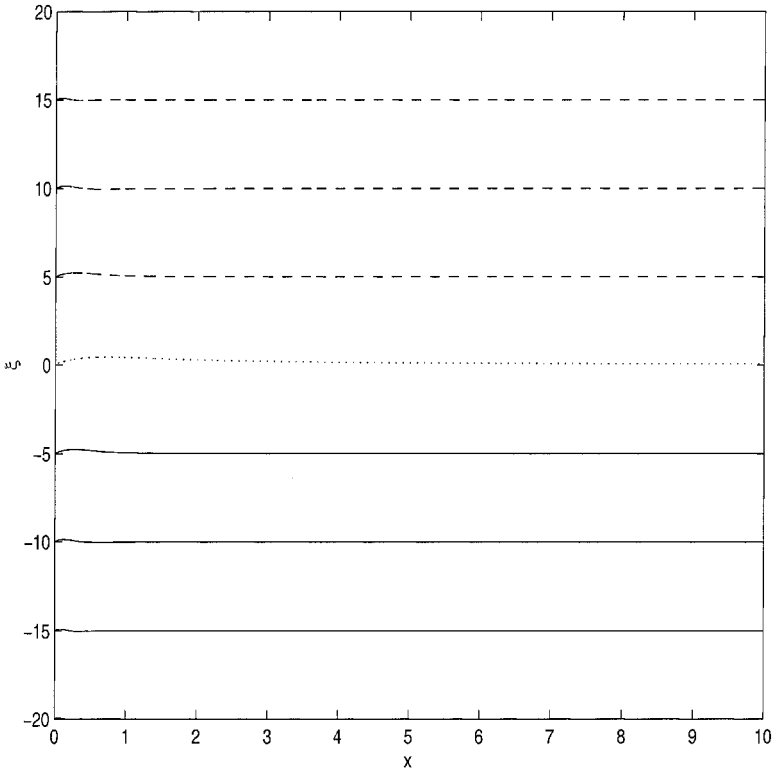

Figure 7. The streamfunction for $\mathsf{T} = 10$. At this value, the perturbations are noticeable, but there is not a significant change of structure. The same contour levels are used as in Figure 6.

the perturbation streamfunction decays, as in Section 3. This is because the y/H lines converge here, and so the effect of diffusion becomes strong, eventually wiping out the perturbation streamfunction entirely.

Therefore, in the equatorial corner, the streamfunction is the same as it was in Section 3. This means that, on streamlines leaving the equatorial corner, the temperature of the fluid T is zero if $\psi > 0$ and $-\mathscr{T}$ if $\psi < 0$, consistent with (4.2).

This fact enables us to interpret the streamlines shown in Figure 9. At $x = 0$, all the contours shown originate from $\xi = -\psi$. The negative contours, carrying cold fluid, run to the north at small values of x, corresponding to a northward displacement of the subpolar gyre. They then follow the direction of decreasing y/H, until they recover their initial value of ξ, at which point they depart from the region of the front (with a slight over-shoot, particularly visible in the most negative contour shown in Fig. 9) and flow out to the deep ocean.

Contours corresponding to small positive values of ψ, carrying warm fluid, behave in a similar way, on the other side of the front, for small values x. They cannot, however, remain close to the front as it approaches the deep water, since the solution would not then match

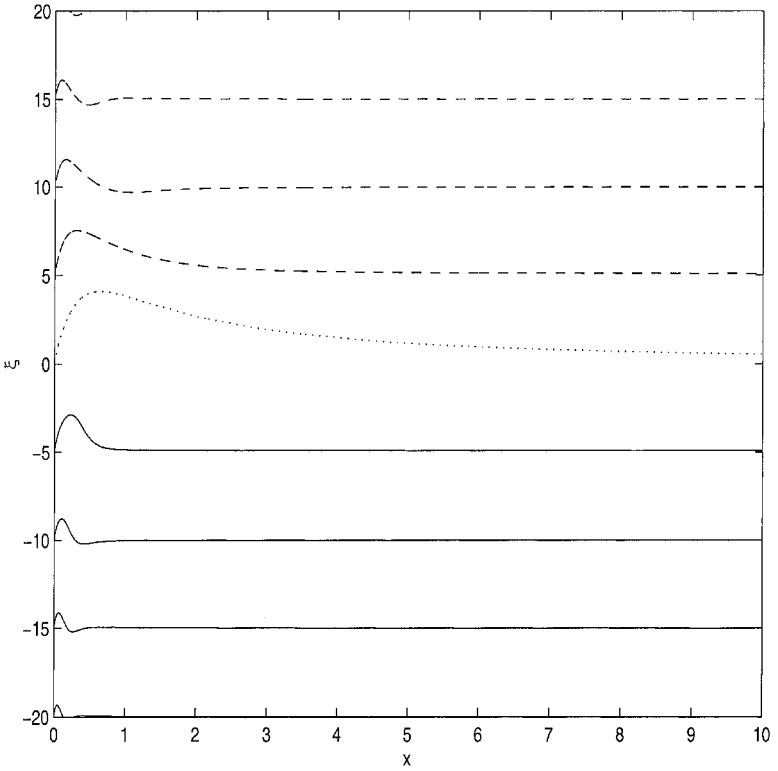

Figure 8. The streamfunction for $\mathsf{T} = 10^2$. At this value, contours of small positive values of ψ are becoming significantly distorted on the slope. The same contour levels are used as in Figure 6.

smoothly to the deep-ocean solution, in which there are no sharp gradients of ψ. Instead, these positive contours depart from the southern flank of the front at some value of $\xi > 0$ and return toward the equatorial corner. Near the corner, they flow in the direction of decreasing ξ, and then flow out to the deep ocean, with $\xi \to -\psi$ as $x \to \infty$, consistent with conditions of matching to the streamfunction in the deep ocean.

For larger positive values of ψ, however, the contour that originates at $x = 0$ does not follow a path that takes it close to the front. Instead, it remains close to its initial value of ξ throughout, and takes the form of a relatively straight open contour that extends from $\xi = -\psi$ at $x = 0$ to $\xi \to -\psi$ as $x \to \infty$. The contour with the critical value of ψ that distinguishes these two cases thus encloses a region to the south of the front and, within this region, a set of closed contours exists for values of ψ larger than this critical value. These closed contours form the gyre that is visible in Figure 9.

A similar pattern of streamlines is illustrated in Figure 10 for $\mathsf{T} = 10^4$. Here we see that a thin boundary layer appears to have formed in the neighborhood of the contour $\psi = 0$. Across this boundary layer, ψ appears to be discontinuous. Elsewhere, it appears that

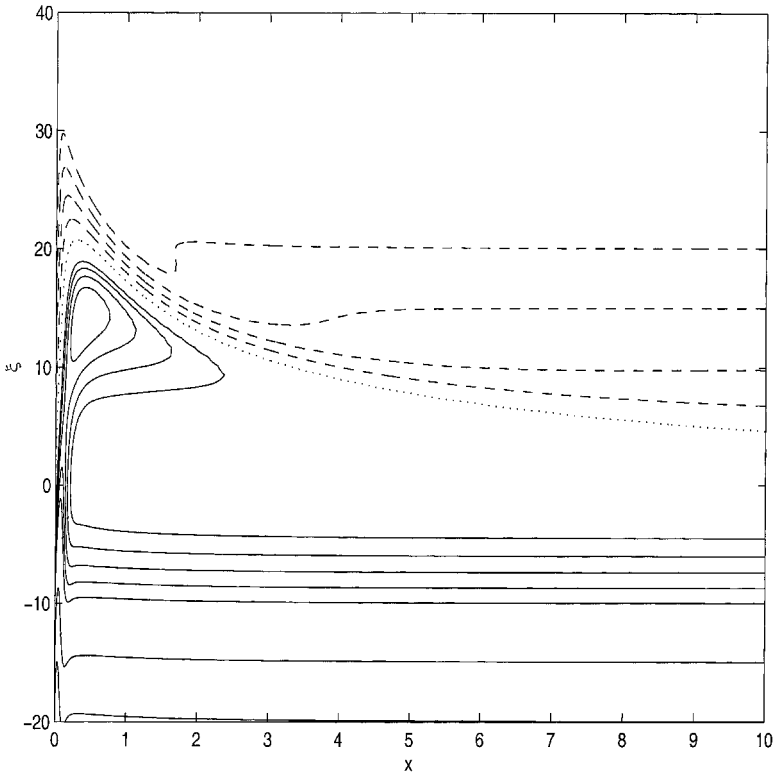

Figure 9. The streamfunction for $\mathsf{T} = 10^3$. At this value, a gyre has formed on the slope in warm water to the south of the contour $\psi = 0$. The contour levels used in 6 are used, but additional positive contour levels between 5 and 10 are shown, with an interval of 1.25, in order to demonstrate the existence of closed contours to the south of the front.

contours of ψ are almost parallel, except close to $x = 0$. The gyre that is present in Figure 9 is also present here, but its center is shifted toward $x = 0$.

To examine this more closely, the streamlines for $\mathsf{T} = 10^4$ are re-drawn in Figure 11, with the range of x restricted to $0 < x < 0.25$. Three solid contours ($\psi = 5, 10, 15$) follow the front from the corner out toward the deep ocean. These contours eventually leave the front and return to the domain of Figure 11 as the first three solid contours that enter the domain above $\xi = 0$ at $x = 0.25$. They then turn around and head back out to the deep ocean in $\xi < 0$. On the other hand, for $\psi \geq 20$ the contours immediately to the south of the front do not originate from $x = 0$, but are in fact closed contours. The open contours with corresponding values of ψ originate from $x = 0$. The contours enter and leave the domain between $0 < x < 0.05$, and run from the equatorial corner to the deep ocean without following the path of the front.

The computational resources required increase as T increases, due to the presence of the thin boundary layer that is evident in the neighborhood of the front in Figure 10. Therefore,

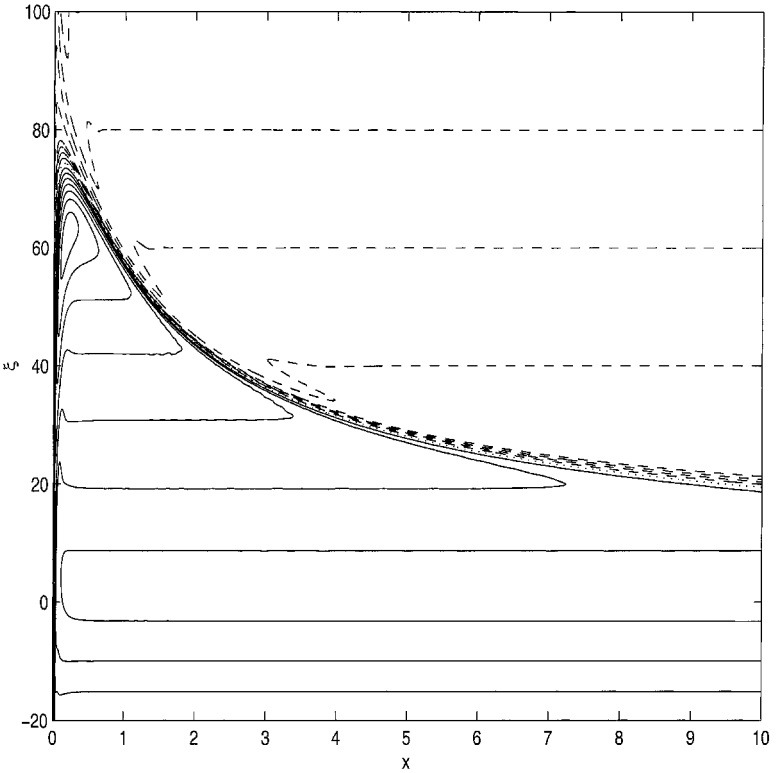

Figure 10. The streamfunction for $\mathsf{T} = 10^4$. The gyre remains on the slope in warm water to the south of the contour $\psi = 0$. For this value of T, a region has formed in the neighborhood of the front in which ψ varies rapidly in the cross-front direction. This variation is much more pronounced in this figure than in Figure 9. Positive contour levels are 5 to 40 with an interval of 5; negative contour levels are -5 to -20 with an interval of 5, and -20 to -100 with an interval of 20.

in the next section, we investigate the limit $\mathsf{T} \to \infty$ analytically. This limit must be consistent with the limit $\mathscr{T} \to 0$ in the case of order-one values of $\mathscr{T}$, and so understanding the limit $\mathsf{T} \to \infty$ helps us to understand the structure of the solution when $\mathscr{T}$ is allowed to be of order unity, at least if $\mathscr{T}$ is not too large.

b. The limit $\mathsf{T} \to \infty$

To analyze the limit $\mathsf{T} \to \infty$, two approaches are possible. Using T as the (large) asymptotic parameter, one approach is to proceed by asymptotic analysis of solutions of (4.6), and the corresponding reconstruction of ψ by (4.4). The other is to analyze Eq. (4.3) for large T. In fact, both approaches are useful: one to connect the analysis to the numerical solutions presented in Section 4a; the other to relate the analysis to that which will be presented in Section 5.

Proceeding first from Eq. (4.6), we can see that, as $\mathsf{T} \to \infty$, ξ_0 must become large. Then, if $\xi_0'(\rho) \neq 0$, there are no stationary phase points, and so the principal contribution to the ρ'

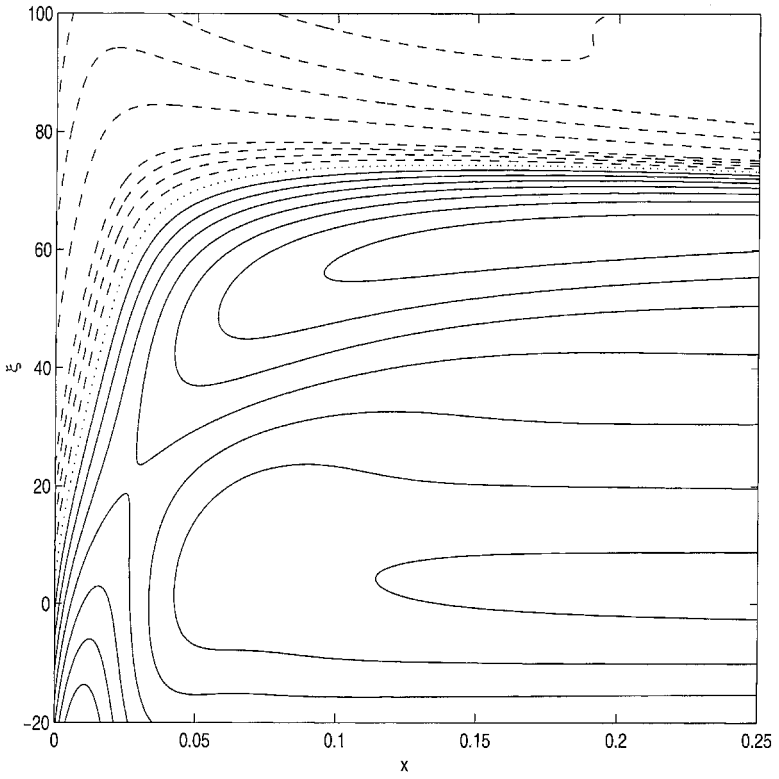

Figure 11. As Figure 10, but for $0 < x < 0.25$.

integral in (4.6) must come from the neighborhood of $\rho' = \rho$, where $\xi_0(\rho) - \xi_0(\rho')$ is smallest, and hence

$$\xi_0(\rho) = \frac{\mathsf{T}}{4\pi}\frac{dH}{d\rho}\int_{-\infty}^{\infty} dk \int_0^{\infty} \exp\{[-ik\xi_0'(\rho) - k^4]u\}\, du. \tag{4.7}$$

The integral in (4.7) can now be evaluated by standard methods. The result is

$$\xi_0(\rho) = \begin{cases} \dfrac{\mathsf{T}}{2}\dfrac{dH}{d\rho}\dfrac{2}{3}\left(-\dfrac{d\xi_0}{d\rho}\right)^{-1} & \text{if} \quad \dfrac{d\xi_0}{d\rho} < 0 \\ \dfrac{\mathsf{T}}{2}\dfrac{dH}{d\rho}\dfrac{1}{3}\left(\dfrac{d\xi_0}{d\rho}\right)^{-1} & \text{if} \quad \dfrac{d\xi_0}{d\rho} > 0 \end{cases}. \tag{4.8}$$

Eq. (4.8) can be integrated, with condition $\xi_0 \to 0$ as $H \to 1$. Only the former choice, $d\xi_0/d\rho < 0$, yields a real solution for ξ_0:

$$\xi_0 = \left[\frac{2\mathsf{T}(1-H)}{3}\right]^{1/2}. \tag{4.9}$$

The latter choice, $d\xi_0/d\rho > 0$, yields an expression for ξ_0^2 which is negative as $H \to 0$. This latter choice is clearly unacceptable, since this solution must be valid as we approach the equatorial corner, in which $H \to 0$.

Note that the co-ordinate ρ does not appear in (4.9). This means that this result is true for any topography $H(x, y)$, provided that $H = 0$ at the coast and $H \to 1$ in the deep ocean. Note also that, in the limit $\mathsf{T} \to \infty$, $\xi_0 = O(\mathsf{T}^{1/2})$, consistent with the observation that the front is deflected more for larger values of T. From (4.9), the maximum value of ξ_0 occurs in the limit $H \to 0$, and the value is $(2\mathsf{T}/3)^{1/2}$. For $\mathsf{T} = 10^3$, this value is 25.8, and for $\mathsf{T} = 10^4$ it is 81.6. These values agree well with maximum departure of the contour $\psi = 0$ from the axis $\xi = 0$ in the numerical solutions shown in Figures 9 and 10, respectively.

The solution (4.9) implies that, as $\mathsf{T} \to \infty$, the front extends across a region in which ξ, and hence ψ, are of magnitude $O(\mathsf{T}^{1/2})$. This solution can also be derived by re-scaling (4.3), and solving a matched asymptotic problem. The re-scaling required is indicated by (4.9), in which we see that both ξ and ψ will be $O(\mathsf{T}^{1/2})$. We therefore replace ψ and ξ in (4.3) by $\mathsf{T}^{1/2}\hat{\psi}$ and $\mathsf{T}^{1/2}\hat{\xi}$, so that $\hat{\psi}$ and $\hat{\xi}$ will remain of order unity as $\mathsf{T} \to \infty$. When this scaling is used in (4.10), the result is

$$\frac{\partial \hat{\psi}}{\partial \rho} + \frac{1}{2}\frac{dH}{d\rho}\,\delta(\hat{\xi} - \hat{\xi}_0(\rho)) = \mathsf{T}^{-2}\frac{\partial^4 \hat{\psi}}{\partial \hat{\xi}^4}. \tag{4.10}$$

The factor T^{-2} in front of the terms with the highest derivatives in (4.10) shows that, for large values of T, the effects of viscosity are confined to boundary layers. This is to be expected. The scaling $\mathsf{T} = O(1)$ was derived to achieve a balance between advection, diffusion and JEBAR. In the limit $\mathsf{T} \to \infty$, we should expect to obtain a limit in which advection and JEBAR are the dominant terms, except in boundary layers where friction may be important.

In (4.10), a boundary layer is expected in the neighborhood of the front at $\hat{\xi} = \hat{\xi}_0(\rho)$. To investigate the solution in such a boundary layer, we define local tangential and normal co-ordinates s and n, defined such that the Jacobian of the transformation between $(\rho, \hat{\xi})$ co-ordinates and (s, n) co-ordinates is unity. The front takes a path $(\rho, \hat{\xi}) = (\rho_0(s), \hat{\xi}_0(s))$, and in the neighborhood of the front the normal derivative of $\hat{\psi}$ is assumed to be large relative to its tangential derivative. Thus the derivative of $\hat{\psi}$ with respect to ρ is approximated as

$$\frac{\partial \hat{\psi}}{\partial \rho} \approx -\frac{d\hat{\xi}_0}{ds}\frac{\partial \hat{\psi}}{\partial n} \tag{4.11}$$

and similarly the derivative of $\hat{\psi}$ with respect to $\hat{\xi}$ is approximated as

$$\frac{\partial \hat{\psi}}{\partial \hat{\xi}} \approx \frac{d\rho_0}{ds}\frac{\partial \hat{\psi}}{\partial n} \tag{4.12}$$

and so

$$-\frac{d\hat{\xi}_0}{ds}\frac{\partial\hat{\psi}}{\partial n}+\frac{1}{2}\frac{dH}{ds}\delta(n)=\mathsf{T}^{-2}\left(\frac{d\rho_0}{ds}\right)^4\frac{\partial^4\hat{\psi}}{\partial n^4}. \tag{4.13}$$

Except at $n=0$, the fundamental solutions to (4.13) are

$$\hat{\psi}=\exp(\mathsf{T}^{2/3}a(s)n), \qquad \text{where} \qquad a=0,\alpha(s)e^{2in\pi/3}, \qquad \text{for} \qquad n=0,\pm1 \tag{4.14}$$

where

$$\alpha(s)=\left[-\left(\frac{d\rho_0}{ds}\right)^4\left(\frac{d\hat{\xi}_0}{ds}\right)^{-1}\right]^{1/3}. \tag{4.15}$$

These solutions must then be combined in order to satisfy matching conditions. In the limit $n\to\infty$, we must approach the deep-ocean value of $\hat{\psi}=-\hat{\xi}$, and in the limit $n\to-\infty$ they must remain bounded. Consequently, $\hat{\psi}$ must take the form

$$\hat{\psi}=\begin{cases}-\hat{\xi}_0(s)+A(s)\exp[\alpha(s)e^{2\pi i/3}\mathsf{T}^{2/3}n] & \\ \quad +B(s)\exp[\alpha(s)e^{-2\pi i/3}\mathsf{T}^{2/3}n] & \text{for} \quad n>0\\ C(s)+D(s)\exp[\alpha(s)\mathsf{T}^{2/3}n] & \text{for} \quad n<0\end{cases} \tag{4.16}$$

Continuity of the first two normal derivatives of $\hat{\psi}$ at $n=0$ yields

$$A(s)=B(s)=-D(s). \tag{4.17}$$

The jump condition on the third derivative can be obtained by integrating (4.13) across $n=0$. It is

$$\frac{1}{2}\frac{dH}{ds}=\mathsf{T}^{-2}\left(\frac{d\rho_0}{ds}\right)^4\left[\frac{\partial^3\hat{\psi}}{\partial n^3}\right]_{n=0^-}^{n=0^+}. \tag{4.18}$$

Using (4.16), the jump condition (4.18) implies

$$\frac{1}{2}\frac{dH}{ds}=-3A\frac{d\hat{\xi}_0}{ds}. \tag{4.19}$$

All of the results derived so far apply to the streamfunction on either side of any front, moving or stationary, over a continental slope. However, in this paper we assume that the flow is steady, and the front is generated by confluence of fluid of different temperatures in the equatorial corner region. Therefore, the front, which is at $n=0$, must coincide with the streamline $\hat{\psi}=0$, and this implies

$$\hat{\xi}_0-\frac{1}{3}\frac{dH}{ds}\left(\frac{d\hat{\xi}_0}{ds}\right)^{-1}=0. \tag{4.20}$$

The solution to (4.20) that is consistent with $d\hat{\xi}_0/ds < 0$ is

$$\hat{\xi}_0 = \left[\frac{2(1-H)}{3}\right]^{1/2}, \tag{4.21}$$

and

$$\hat{\psi} = \begin{cases} -\hat{\xi}_0(s)[1 - \exp(-\mathsf{T}^{2/3}\alpha(s)n/2)\cos(\sqrt{3}\mathsf{T}^{2/3}\alpha(s)n/2)] & \text{for} \quad n > 0 \\ \tfrac{1}{2}\hat{\xi}_0(s)[1 - \exp(\mathsf{T}^{2/3}\alpha(s)n)] & \text{for} \quad n < 0 \end{cases} \tag{4.22}$$

The solution (4.21) for the location of the front, obtained above by direct analysis of the equations of motion, agrees with the solution (4.9) obtained by asymptotic analysis of the integral (4.6), on recalling that $\xi_0 = \mathsf{T}^{1/2}\hat{\xi}_0$.

The solution (4.22) is valid on the boundary-layer scale $n = O(\mathsf{T}^{-2/3})$, where n measures distance from the front. At $n = 0$, the solution (4.22) takes the value $\hat{\psi} = 0$, which would also be the case if this boundary layer was attached to a wall. In the direction of the deep ocean ($n > 0$) the boundary layer solution approaches the value of $\hat{\psi}$ that corresponds to the value that $\hat{\psi}$ takes on this value of y/H due to the action of wind forcing in the deep ocean. In fact, these values of $\hat{\psi}$ are negative, reminding us that these values of y/H correspond to the subpolar gyre. Between the front and the deep ocean, the structure of the solution is oscillatory. This oscillatory behavior is visible in the numerical solution shown in Figure 10, where it can be seen that, on the deep ocean side of the front, the streamfunction oscillates as it approaches the front.

In a boundary layer attached to a vertical wall (Munk, 1950), either $\hat{\psi}_n$ or $\hat{\psi}_{nn}$ would also be zero at $n = 0$. Here, however, the continuity conditions and jump condition (4.18) together imply that, on the other side of the front (i.e. in $n < 0$), $\hat{\psi}$ tends without oscillation to $\tfrac{1}{2}\hat{\xi}_0$ as $n \to -\infty$; i.e. to a value that is one-half in magnitude, and opposite in sign, to the value taken in the deep ocean. Thus, away from the front, $\hat{\psi}$ is given by

$$\hat{\psi} = \begin{cases} -\hat{\xi} & \text{for} \quad \hat{\xi} > \hat{\xi}_0(\rho) \quad \text{or} \quad \hat{\xi} < 0 \\ \tfrac{1}{2}\hat{\xi} & \text{for} \quad 0 < \hat{\xi} < \hat{\xi}_0(\rho) \end{cases}. \tag{4.23}$$

We can see that, away from the equatorial corner, and away from the front, the numerical solution for $\mathsf{T} = 10^4$ displayed in Figure 10 agrees well with (4.23).

Thus far, we have seen that the solution obtained by consideration only of the main shelf region $r = O(1)$ consists of contours of $\hat{\psi}$ co-incident with lines of constant $\hat{\xi}$, except within a boundary layer centered on the front, across which the value of $\hat{\psi}$ jumps from $-\hat{\xi}$ on the northern side to $\tfrac{1}{2}\hat{\xi}$ on the southern side. This structure can clearly be seen in the numerical solution in Figure 10. The solution is valid for $\rho = O(1)$, but inconsistent with the analyses in the limits $\rho \to \pm\infty$ presented in Appendices B and C. Moreover, we know that $\hat{\psi} \to -\hat{\xi}$ as $r \to 0$, and this is clearly not satisfied by this solution at $x = 0$ between $\hat{\xi} = 0$ and $\hat{\xi} = (2/3)^{1/2}$. In both of these limits, regions exist in which no approximation is possible to the

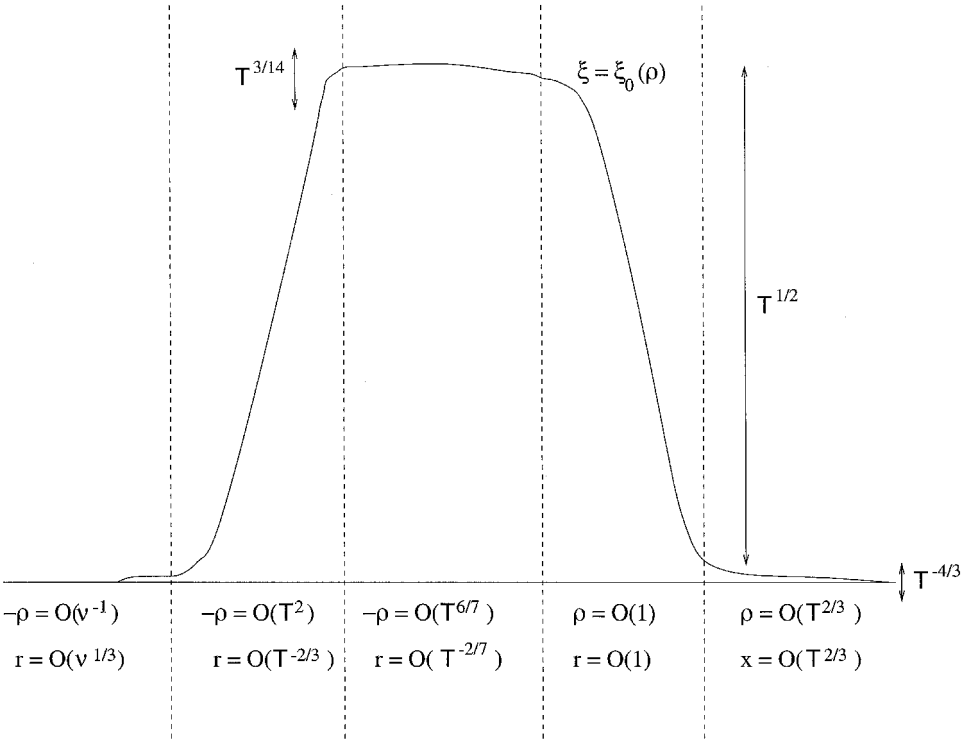

Figure 12. The asymptotic regions in the limit $T \to \infty$. The solid line indicates schematically the solution $\xi = \xi_0(\rho)$.

leading-order contribution to the integral in (4.9) and so essentially the full Stefan-type problem returns, and $\hat{\xi}_0$ (and hence $\hat{\psi}$) must be determined numerically. The need for additional asymptotic regions to describe the solution completely is apparent in Figure 11, where we see that the contours of $\hat{\psi}$ do not remain straight all the way to $x = 0$.

In fact, we find that three additional regions are required. In the limit $\rho \to \infty$, one region is required, in which $\rho = O(T^{2/3})$. In this region $\xi = O(T^{-4/3})$. This is required because, at large x, the ocean floor becomes flat and so, although the front is still present, there is no JEBAR. This outer region describes how JEBAR is initially turned on at large values of x, and so in this region all terms are equally significant. In the limit $\rho \to -\infty$, two regions are required. One is a full Stefan region, $(-\rho) = O(T^{6/7})$, and in this region ξ varies by an amount $\Delta\xi = O(T^{3/14})$. The other is a region in which $\Delta\xi = O(T^{1/2})$ and $(-\rho) = O(T^2)$, which is required to allow the perturbation streamfunction to diffuse and so for ψ to return to its deep-ocean value $-\xi$ as we approach the corner $r = O(\nu^{1/3})$. The asymptotic structure is summarized in Figure 12.

Now, in Figures 9 and 10 we saw that, for small positive values of ψ, there is a single contour that originates in the equatorial corner, and initially follows a path just to the south of the front. The solution for ψ in the region $(-\rho) = O(T^2)$, shown in Figure 13, enables us

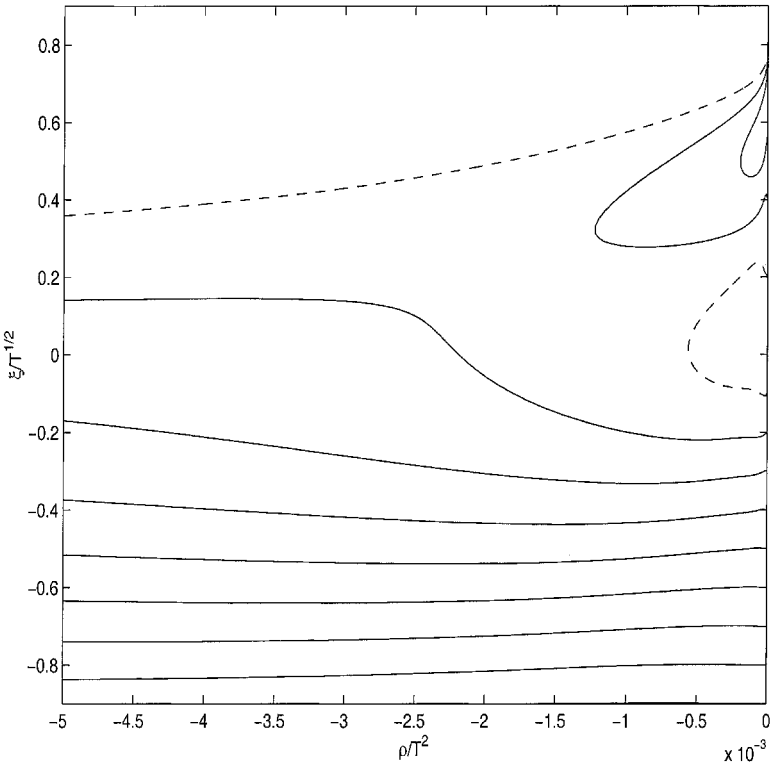

Figure 13. Contours of positive values of ψ in $\rho < 0$. The contour interval is $0.1T^{1/2}$. The contours of $\psi = 0.1T^{1/2}$ are dashed, and all other contours are solid.

to describe this aspect of the solution in the limit $T \to \infty$. We see in Figure 13 that, for $\psi = 0.1T^{1/2}$, the contour that originates from $\xi = -0.1T^{1/2}$ as $\rho \to -\infty$ enters the domain at about $\xi = 0.35T^{1/2}$. It leaves the region $\rho < 0$ at $\xi = (2T/3)^{1/2} \approx 0.816T^{1/2}$, which corresponds to the location of the front. This corresponds to a contour over the slope that is just to the south of the front. The solution (4.23) implies that this contour departs from the front at $\xi = -2\psi = 0.2T^{1/2}$, and returns to the region shown in Figure 13 in a straight line (in $\rho - -\xi$ space). This is, therefore, the contour that enters the domain shown in Figure 13 at $(\rho, \xi) = (0.0, 0.2T^{1/2})$ and leaves it again at $(0.0, -0.1T^{1/2})$. All this implies that, in the limit $T \to \infty$, the contour $\psi = 0.1T^{1/2}$, and all contours $0 < \psi < 0.1T^{1/2}$, are single contours. Therefore, just to the south of the front, the warm water is continually replenished by advection through the equatorial region from the equatorial deep ocean. In contrast, for larger values of ψ we have one set of contours that has both ends in $0 < \xi < (2T/3)^{1/2}$ on $\rho = 0$, and another set of contours that extend directly from the equatorial corner (left side) to $\xi = -\psi$ at $\rho = 0$. The first set corresponds to the inner end of the closed contours (c.f. Fig. 11), while the second set correspond to the contours of the subtropical gyre. In the first set, contours meet at $\rho = 0$, $\xi = (2T/3)^{1/2}$. This is the location of the center of the

recirculation. The apparent singularity is resolved in the region, previously mentioned, that is of scale $(-\rho) = O(\mathsf{T}^{6/7})$, $\xi = (2\mathsf{T}/3)^{1/2} + \Delta\xi$, where $\Delta\xi = O(\mathsf{T}^{3/14})$. The fluid in the recirculation region is thus surrounded on all sides by fluid of the (warm) temperature of the subtropical gyre and so, by thermal diffusion, it will also take the temperature of the subtropical gyre (Batchelor, 1956), as we have assumed.

The conclusion to be drawn from this section is that, as $\mathsf{T} \to \infty$, the displacement of the contour $\psi = 0$ from the contour $y/H = y_0$ increases at $\mathsf{T}^{1/2}$. This occurs over the main slope region, where $r = O(1)$. The path of the front in this region can be obtained by solving a simple first-order differential equation (4.6). This region is flanked at either end by regions in which a Stefan-type problem must be solved, but the solution in these regions does not affect the path of the front in the region $r = O(1)$. On the approach to the corner region, there is a further region, $-\rho = O(\mathsf{T}^2)$ or, equivalently, $r = O(\mathsf{T}^{-2/3})$, in which $\xi_0(\rho)$ returns to the contour $y/H = y_0$. In this region, streamlines corresponding to small positive values if ψ run from the equatorial corner along the southern side of the front, indicating that the re-circulating anticyclonic gyre on the slope is isolated by a finite distance from the front.

5. The strongly nonlinear regime $\mathscr{T} = O(1)$

We have seen in Section 4b that for large values of T an asymptotic structure develops in which, in the neighborhood of the front, a viscous boundary layer develops. This must be consistent with the structure of the solution for order-unity values of $\mathscr{T}$, at least for small $\mathscr{T}$. In this section, we therefore start by considering the dynamics of a sharp front outside the corner region. Motivated by the solutions presented in Sections 3 and 4, we shall assume that the temperature T satisfies

$$T = \begin{cases} -\mathscr{T} & \text{for} \quad \psi < 0 \\ 0 & \text{for} \quad \psi > 0 \end{cases} \tag{5.1}$$

and there is a thermal boundary layer, or front, in the neighborhood of $\psi = 0$ that is thinner than any corresponding viscous boundary layer in ψ. This assumption must be valid for small values of $\mathscr{T}$, since in that limit it must be consistent with the solution already presented in Section 4. The assumption is verified by the following analysis for larger values of $\mathscr{T}$, but we shall see that there is an upper bound on the value of $\mathscr{T}$.

Following the analysis presented in Section 4b, the front introduces a small scale normal to itself, and a viscous boundary layer, of width $O(\nu^{1/3})$, is required about the front. The equation for ψ in such a layer is

$$-\frac{d(y/H)}{ds}\frac{\partial\psi}{\partial n} + \frac{\mathscr{T}}{2}\frac{dH}{ds}\delta(n) = \frac{\nu}{H}\frac{\partial^4\psi}{\partial n^4}. \tag{5.2}$$

Here, n is the normal co-ordinate, with the front at $n = 0$, and s is the length along the front, measured from the corner $r = 0$. The viscous boundary layer is taken to be sufficiently thin

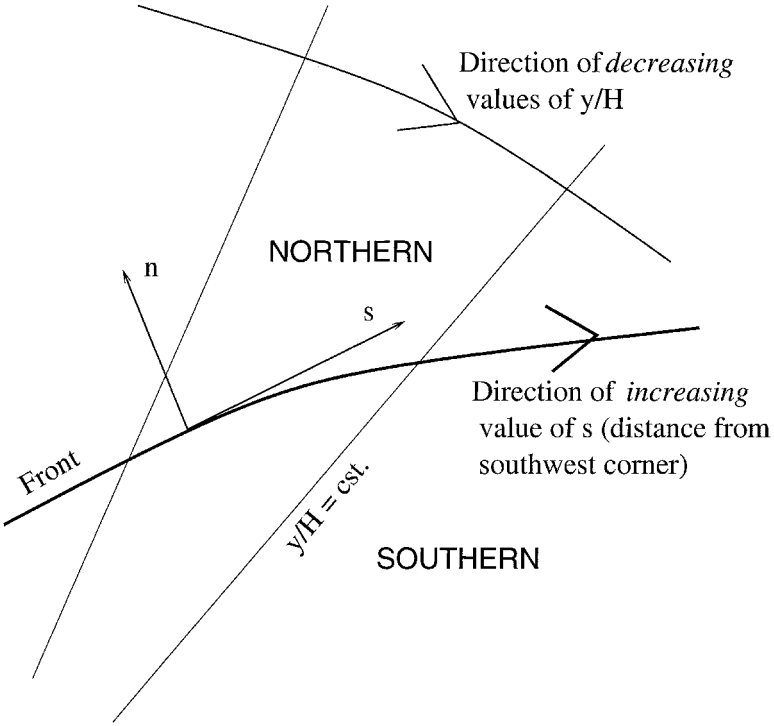

Figure 14. A schematic diagram showing the path of the front, together with two typical contours of y/H. The northern and southern sides of the front are shown. Here, "northern" means the side on which the contours of y/H extend to the deep ocean, whereas "southern" means the side on which the contours of y/H extend to the southwest corner.

that variations of y and H across it are negligible, so in (5.2) y and H are functions of s. Eq. (5.2) is the analogue of (4.13).

It follows from (5.2) that, except at $n = 0$, ψ takes the form

$$\psi = \exp(a(s)n), \qquad \text{where} \qquad a = 0, \alpha(s)e^{2in\pi/3} \qquad \text{for} \qquad n = 0, \pm 1 \tag{5.3}$$

and where

$$\alpha(s) = \left(-\frac{H}{\nu} \frac{d(y/H)}{ds} \right)^{1/3}. \tag{5.4}$$

We suppose, as required for consistency with the results of Section 4b, that $d(y/H)/ds < 0$, so $\alpha(s)$ is real (we must verify *a posteriori* that our solution remains consistent with this supposition for all values of $\mathscr{T}$). In the direction $n > 0$ contours of y/H extend to the deep ocean, and in the direction $n < 0$ they extend to the southwestern corner. The situation is depicted in Figure 14.

The fluid is of uniform temperature on either side of the front, and therefore, away from the viscous boundary layer, ψ is a function of y/H. It follows that, on the northern side of

the front, at a given value of y/H, the streamfunction ψ must take its deep ocean value $\Psi(y/H)$. On the southern side we require that ψ must remain bounded far from the front, but the value of ψ is determined as part of the solution. This value of ψ is then propagated along the y/H characteristic to the equatorial corner, where y/H contours meet and viscosity acts to remove conflicts.

Thus, we require $\psi \to \Psi(y/H)$ as $n \to \infty$, and ψ and its first two normal derivatives to be continuous at $n = 0$. A jump condition on the third normal derivative of ψ can be obtained by integrating (5.2) from $n = 0^-$ to $n = 0^+$. The result is

$$\left[\frac{\partial^3 \psi}{\partial n^3}\right]_{n=0^-}^{n=0^-} = \frac{\mathscr{T} H}{2\nu} \frac{dH}{ds} \tag{5.5}$$

The general solution for ψ consistent with conditions as $n \to \pm\infty$

$$\psi = \begin{cases} A(s) \exp(\alpha e^{2i\pi/3} n) + B(s) \exp(\alpha e^{-2i\pi/3} n) + \Psi(y/H) & \text{for} \quad n > 0 \\ C(s) + D(s) \exp(\alpha n) & \text{for} \quad n < 0 \end{cases} \tag{5.6}$$

Continuity of ψ, ψ_n and ψ_{nn} at $n = 0$ implies

$$A(s) = B(s) = -D(s); \qquad C = 3A(s) + \Psi(y/H). \tag{5.7}$$

The value of $A(s)$ can now be determined from the jump condition (5.5):

$$A(s) = \frac{\mathscr{T}}{6} \frac{dH}{d(y/H)}. \tag{5.8}$$

In addition, Eq. (2.8b) requires that $\psi = 0$ at $n = 0$, and this implies

$$2A(s) + \Psi(y/H) = 0. \tag{5.9}$$

Eqs. (5.7) and (5.9) imply that, within the viscous boundary layer, ψ is given by

$$\psi = \begin{cases} \Psi(y/H)[1 - e^{-\alpha n/2} \cos(\sqrt{3}\alpha n/2)] & \text{for} \quad n > 0 \\ -\tfrac{1}{2}\Psi(y/H)(1 - e^{\alpha n}) & \text{for} \quad n < 0 \end{cases}. \tag{5.10}$$

From (5.10) we see that the thickness of the boundary layer is given by α^{-1}, which is $O(\nu^{1/3})$, and also that $\psi \to -\tfrac{1}{2}\psi(y/H)$ as $n \to -\infty$. Hence, outside of the viscous boundary layer, we have

$$\psi(x, y) = \begin{cases} \Psi(y/H) & \text{if} \quad y/H < y_0 \quad \text{or} \quad y/H > y_0 \\ & \quad \text{and } (x, y) \text{ is to the north of the front} \\ -\tfrac{1}{2}\Psi(y/H) & \text{if} \quad y/H > y_0 \quad \text{and } (x, y) \text{ is to the south of the front} \end{cases} \tag{5.11}$$

Eq. (5.11) is the analog of the result (4.23) of Section 4b.

To obtain the path taken by the front, we use Eqs. (5.8) and (5.9) to see that the location of the front must satisfy

$$3\Psi(y/H)d(y/H) - \mathscr{T}dH = 0 \tag{5.12}$$

Eq. (5.12) can be integrated to give

$$3\int_{y_0}^{y/H} \Psi(q)\,dq + \mathscr{T}(1 - H) = 0 \tag{5.13}$$

where y_0 is the latitude in the deep ocean ($H = 1$) at which $\psi = 0$. Again, as in Section 4b, there is no explicit dependence on arc length, and no special conditions on Ψ or H, except that there must be no closed contours of y/H, and Ψ must have a classical double-gyre form. Moreover, given that Ψ has a classical double-gyre form, with $\Psi(q) < 0$ for $q > y_0$, and *vice versa,* it follows from (5.13) that the value of y/H decreases as the distance from the southwest corner increases. Thus, this solution is consistent with the assumption $d(y/H)/ds < 0$. The alternative assumption, $d(y/H)/ds > 0$, leads to path equation which does not have a real solution for y/H as $H \to 0$, even for small values of $\mathscr{T}$.

In Figure 15 we show the form of $\psi(x, y)$ when $\mathscr{T} = 0$; i.e., a homogeneous ocean with no temperature difference between subpolar and subtropical gyres, for the particular choice of $\lambda = 1$, $y_0 = 1$ and $\Psi(q)$ given by

$$\Psi(q) = \begin{cases} \sin(\pi q) & \text{for} \quad 0 < q < 2 \\ 0 & \text{for} \quad t > 2\,. \end{cases} \tag{5.14}$$

In this case there is no front, and the streamlines follow the contours of y/H to the equatorial corner, where a region in which viscosity is significant is formed, as discussed in Section 3.

With $\Psi(q)$ given by (5.14), Eq. (5.13) is

$$\mathscr{T}(1 - H) = \begin{cases} \dfrac{3}{\pi}\left[\cos(\pi y/H) + 1\right] & \text{for} \quad y/H \le 2 \\ \dfrac{6}{\pi} & \text{for} \quad y/H > 2 \end{cases}. \tag{5.15}$$

In Figure 16 we present the streamfunction $\psi(x, y)$ for the case $\mathscr{T} = 0.95$. Note here that, in comparison with the case $\mathscr{T} = 0$, the subpolar gyre does not extend so far to the south on the continental slope, except in very shallow water. Instead, the flow in the subpolar gyre returns to deep water on the northern side of the front in a region of thickness $O(\nu^{1/3})$. We do not depict such a thin layer in Figure 16, and so ψ appears discontinuous at the location of the front.

Note also that the contour $y/H = 1$ is a local minimum value of ψ (at which $\psi = 0$ according to 5.11) as indicated by the two dashed lines, which are contours of $\psi = 0.05$. In the region between the contour $y/H = 1$ and the front the value of ψ increases to the north and, just south of the front, the value of ψ is $-\frac{1}{2}\Psi(y/H)$. As in the limit $\mathsf{T} \to \infty$ presented

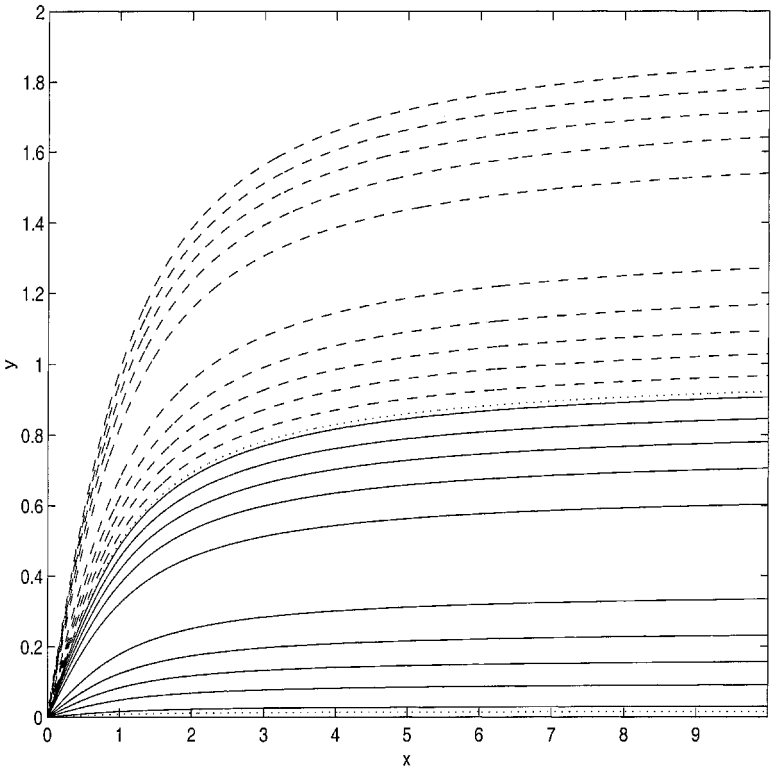

Figure 15. Contour plot of ψ on the continental slope for a barotropic ocean. Solid contours are levels $\{0.1, 0.3, 0.5, 0.7, 0.9\}$, corresponding to the subtropical gyre, while dashed contours are levels $\{-01, -0.3, -0.5, -0.7, -0.9\}$, corresponding to the subpolar gyre. The dotted contour is 0.05.

in Section 4b, the contours immediately to the south of the front are long extended open contours forming part of the sub-tropical gyre, whereas those with larger values of ψ form a region of anticyclonic recirculation on the shelf. In this case the value of ψ to the south of the front increases as we approach the equatorial corner, and so the centre of anticyclonic recirculation is to be found on some scale $r \ll 1$.

In Figure 17 we present the streamfunction in the viscous boundary layer for the case $\mathscr{T} = 0.95$. We see that the strength of flow in this viscous boundary layer decreases with increasing distance from the corner. Thus, in this case, the strength of the thin baroclinic current is greatest at the equator, and decreases monotonically as the front flows across the slope.

In Figure 18 we present the streamfunction $\psi(x, y)$ for the case $\mathscr{T} = 1.9$. Again, there is clearly a region of anticyclonic recirculation between the front and the main part of the subtropical gyre. Here, however, the maximum value of ψ south of the front occurs at the value of y/H that corresponds to the centre of the subpolar gyre and so, in this case, the

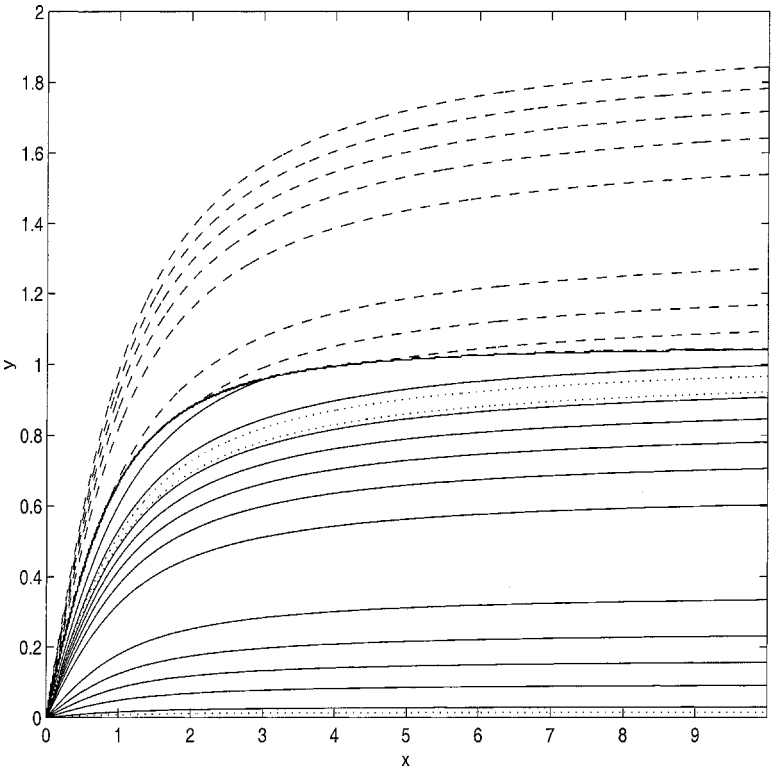

Figure 16. Contour plot of ψ on the continental slope for a baroclinic ocean with $\mathscr{T} = 0.95$. The contour levels are the same as in Figure 15.

center of the anticyclonic recirculation region occurs away from the corner region, with co-ordinates $y/H = 1.5 = y_1$, say, and hence, by (5.15), $H = 1 - 3/(\pi.\mathscr{T})$. The value of ψ at the center of this re-circulating anticyclonic gyre is $-0.5\Psi(y_1)$.

In Figure 19 we present the streamfunction in the viscous boundary for the case $\mathscr{T} = 1.9$ (we shall see that the maximum allowed value of $\mathscr{T}$ is $6/\pi \approx 1.9099$). In contrast to the case $\mathscr{T} = 0.95$ shown in Figure 17, here we observe that closed gyres are present in the solution to the north of the front.

The location and strength of these gyres can be determined analytically from (5.10). For local extrema of ψ (and hence closed contours) to exist, we require $\psi_n = 0$ and $\psi_s = 0$. For $n > 0$ we have $\psi_n = 0$ if $\tan(\sqrt{3}\alpha n/2) = -1/\sqrt{3}$. Thus, there are infinitely many $n > 0$ that satisfy this condition. In contrast, we cannot have $\psi_n = 0$ for $n \leq 0$, except when $\Psi(y/H) = 0$. The condition $\psi_s = 0$ then requires $\Psi'(y/H) = 0$. For a $\Psi(y/H)$ that corresponds to a classical double-gyre circulation, the condition $\Psi'(y/H) = 0$ occurs for precisely one value of y/H: the value that corresponds to the centre of the sub-polar gyre, which we have denoted by $y/H = y_1$.

Hence, in the viscous boundary layer, there are an infinite number of gyres, of alternating

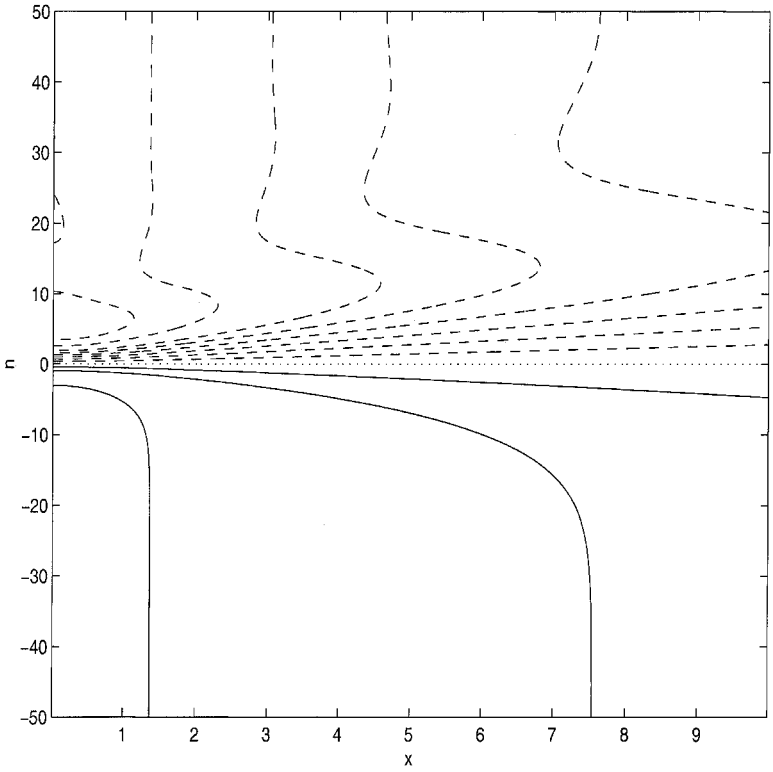

Figure 17. The streamfunction in the viscous boundary layer, $\mathscr{T} = 0.95$. The normal co-ordinate n has been re-scaled on $\nu^{1/3}$.

sign, of which the largest is cyclonic, to the north of the front. These recirculating gyres are all centered on the location along the front at which $y/H = y_1$. The strength of the recirculations decreases exponentially with n, so only the first one or two appear significant in Figure 19. The value of ψ at the center of the first re-circulation shown is $\{1 + (\sqrt{3}/2)\exp[-5\pi/(6\sqrt{3})]\}\Psi(y_1) \approx 1.191\Psi(y_1)$. Of course, this only occurs if $\mathscr{T}$ is sufficiently large that $y/H = y_1$ occurs at some location along the front. In our case, that condition is $\mathscr{T} \geq 3/\pi$. For smaller values of $\mathscr{T}$ (e.g. $\mathscr{T} = 0.95$), no recirculations exist to the north of the front. This is in contrast to the single anticyclonic gyre that exists to the south of the front, outside the viscous boundary layer, for all values of $\mathscr{T}$. For $\mathscr{T} < 3/\pi$ the center of the anticyclonic gyre is in $r \ll 1$, but for $\mathscr{T} > 3\pi$ its center is at $y/H = y_1$, in common with the cyclonic gyre to the north of the front. Thus, accounting for both northern and southern recirculations, the total maximum strength of the baroclinic current in our model is $-1.691\Psi(y_1)$.

The condition that the location of the front approaches the equatorial corner region as $H \to 0$ is important for the existence of the solutions presented in this section. This is because we assume that the front forms in the corner region as a result of advection into the

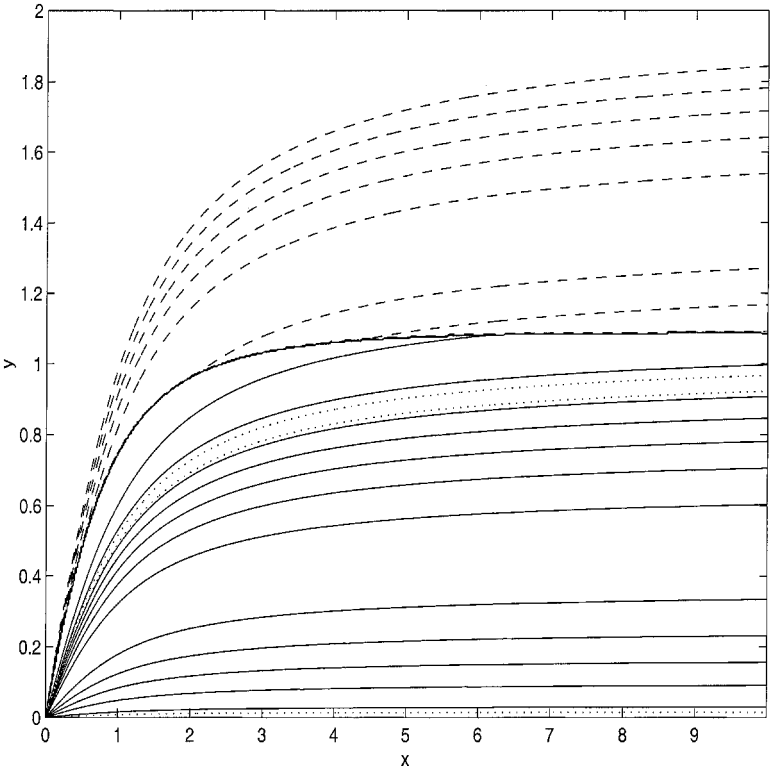

Figure 18. Contour plot of ψ on the continental slope for a baroclinic ocean with $\mathscr{T} = 1.9$. The contour levels are the same as in Figure 15.

corner region of warm water from the subtropical gyre and cold water from the subpolar gyre. Therefore, we require that the path defined by (5.13) must approach the corner $(x, y) = (0, 0)$ as it approaches the coast $H = 0$. This means that, for the validity of the solutions presented here, there must exist some value of $y/H < \infty$ for which a solution to (5.13) exists when $H = 0$. Assuming a classical double-gyre structure, with $\Psi(y) < 0$ for $y > y > y_0$, this condition is

$$\mathscr{T} < -3 \int_{y_0}^{\infty} \Psi(q)\, dq. \tag{5.16}$$

For the solutions presented in this section, with $\Psi(q)$ given by (5.14), the condition (5.16) is

$$\mathscr{T} < \frac{6}{\pi} \approx 1.91. \tag{5.17}$$

As in the analysis of the limit $\mathsf{T} \to \infty$ presented in Section 4b, the solutions presented

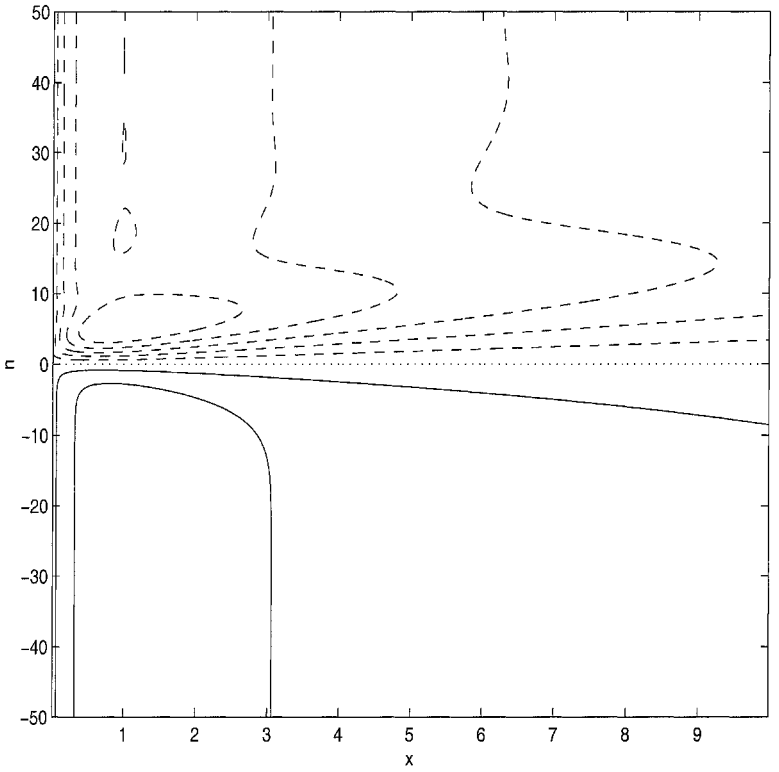

Figure 19. Contour plot of ψ in the viscous boundary layer, $\mathscr{T} = 1.9$. The normal co-ordinate n has been re-scaled on $\nu^{1/3}$.

here become invalid both as $x \to \infty$ (the deep ocean) and as $r \to 0$ (the equatorial corner region) and, as in Section 4b we find that regions are required in both of these limits in which a Stefan-type problem must be solved.

The region $\rho = O(\mathsf{T}^{2/3})$ of Section 4b corresponds to a region $x = O(\nu^{-1/3})$. In Appendix D we show that this region matches to the outer limit of the flow over the slope. The region $-\rho = O(\mathsf{T}^{6/7})$ of Section 4b corresponds to a region $r = O(\nu^{1/7})$. In Appendix E we show that this region matches to the inner limit of the flow over the slope.

One difference does exist between the boundary-layer structure for $\mathscr{T} = O(1)$ and that for $\mathsf{T} = O(1)$: namely, the region $-\rho = O(\mathsf{T}^2)$ corresponds, when $\mathsf{T} = O(\nu^{-1/2})$, to $r = O(\nu^{1/3})$. This means that, although JEBAR is still negligible in the corner region $r = O(\nu^{1/3})$ when $\mathscr{T} = O(1)$, the boundary conditions in the limit $R \to \infty$ are given by (5.11). However, JEBAR is negligible in the corner region even when $\mathscr{T} = O(1)$, and so a front will form as hot and cold fluid is brought together the corner region, just as in Sections 3 and 4. Thus, the assumption of a sharp temperature front over the continental slope is justified, provided condition (5.16) is satisfied.

6. Discussion

The philosophy of this paper was to investigate the effect of the interaction of baroclinicity and topography in the simplest possible baroclinic model of ocean circulation, with particular attention to the western boundary current. In this context, we have studied a model in which temperature is independent of depth, and the sea-surface temperature T and potential energy density γ are related by $\gamma = \frac{1}{2}H^2T$. While this is indeed a severe approximation, it has the virtue of being an exact solution of the three-dimensional equations of motion, and we hope to regard it as a paradigm for models where a more realistic relationship between sea-surface temperature and potential energy exists.

In Sections 3, 4 and 5 we have presented solutions to the nonlinear equations (2.8). However, there is no general theory of (2.8). The analysis presented in Sections 3 and 4 is important, because it shows that the solutions presented in Section 5 develop smoothly from the barotropic solution $\psi = \Psi(y/H)$ as $\mathscr{T}$ is increased, first through small values $\mathscr{T} \ll \nu^{1/2}$, then through moderate values $\mathscr{T} = O(\nu^{1/2})$, and then up to values $\mathscr{T} = O(1)$. While this does not necessarily make these solutions more physically relevant than other possible solutions, it does show that they correspond, when $\mathscr{T} = O(1)$, to the only class of solutions that exists in the familiar barotropic limit $\mathscr{T} \to 0$.

The simplicity of the model notwithstanding, it is interesting to consider the qualitative features of the ocean circulation that these solutions predict. A cartoon of the circulation implied by our analysis when $\mathscr{T} = O(1)$, based on Figures 18 and 19 is shown in Figure 20. We see

1. A strong baroclinic current, or front, flowing to the northwest across the continental slope in a direction of decreasing y/H.
2. A "cut-off" subpolar gyre, which does not extend to the equator, in contrast to the barotropic theory.
3. A region of anticyclonic recirculation to the south of the baroclinic current.
4. A succession of eddies of alternating sign to the north of the baroclinic current, of which the strongest is cyclonic.

All of these features are present, to some extent, in the cartoons of the North Atlantic circulation presented by Schmitz and McCartney (1993), and they are supported by detailed observations. Leaman *et al.* (1989) describe the Gulf Stream as a strong baroclinic current, flowing northward on the western continental slope of the North Atlantic, with y/H decreasing as it flows to the north. Hogg *et al.* (1986) and Hogg (1992) describe recirculation gyres both to the north and south of the Gulf Stream. Hogg (1992) proposes that the transport in each of these gyres is approximately 30–40 Sverdrups.

If the strength of the subpolar gyre in the North Atlantic is assumed to be approximately 30 Sverdrups (i.e. $\Psi(y_1) = -30$ Sverdrups), as suggested by Schmitz and McCartney

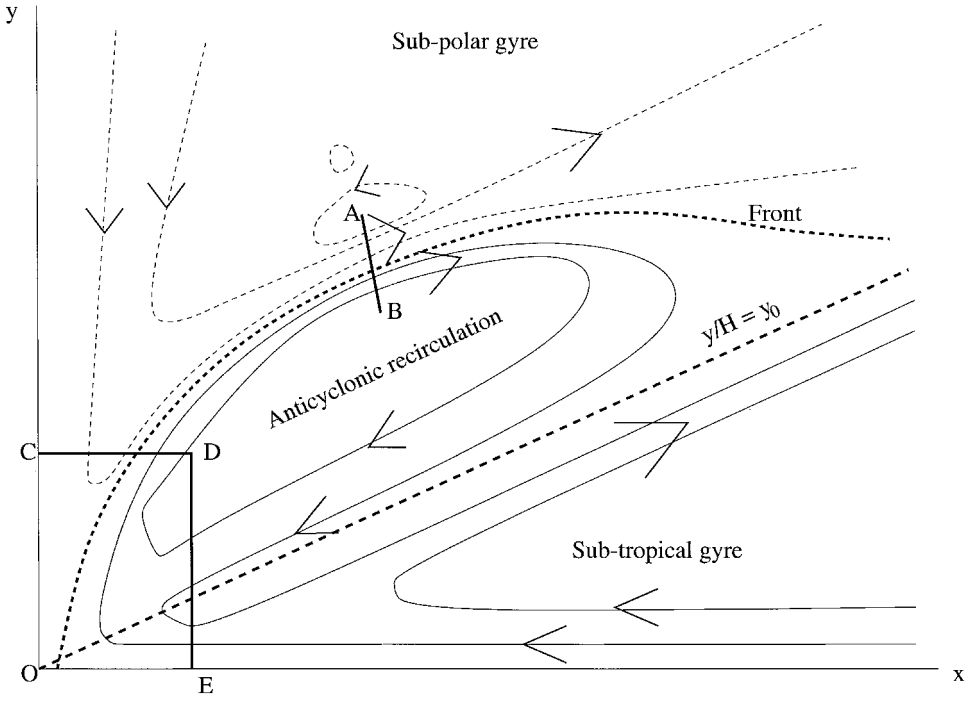

Figure 20. A cartoon of the circulation when $\mathscr{T} = O(1)$. The thin solid lines are positive contours of ψ, and the thin dashed lines are negative contours of ψ. The point A is at the center of the cyclonic recirculation, and the point B is at the center of the anticyclonic recirculation. The length of the line AB is $O(\nu^{1/3})$. The corner region $OCDE$ is of scale $\nu^{1/3} \times \nu^{1/3}$. The region of anticyclonic recirculation lies between the contour $y/H = y_0$ and the front, both depicted as bold dashed lines. The bold arrows indicate the direction of flow.

(1993), then, according to the calculations of Section 5, our southern recirculation gyre has a transport of 15 Sverdrups, and our northern recirculation gyre has a transport of 5.7 Sverdrups. Thus, the total transport of our baroclinic current at its strongest point is 50.7 Sverdrups, compared with the maximum transport in a classical western boundary current in a flat-bottomed ocean of 30 Sverdrups. Although 50.7 Sverdrups is significantly less than the observed transport of the Gulf Stream, which can be over 100 Sverdrups (Leaman *et al.,* 1989; Johns *et al.,* 1995), it suggests that the theory presented here may be at least a partial description of the dependence on the transport of the Gulf Stream with location.

Note that the strength of the baroclinic current, and of the associated recirculation regions, is determined by conditions which depend only on the strength of the subpolar gyre, but are independent of the strength of the subtropical gyre. This may be the least realistic aspect of the present model, indicated in Figure 20 by the fact that all the contours of $\psi > 0$ that are immediately to the south of the front return to the equatorial corner along

the southern boundary of the anticyclonic recirculation region before heading out to the deep ocean.

Most theories of recirculation rely on inertia, and in the present theory this is parameterized, in perhaps a very crude way, by the Laplacian applied to the depth-averaged flow in (2.8a). The strengths of both of the recirculation gyres in this paper are independent of the value of the diffusion parameter ν, which has been assumed to be asymptotically small, but they do depend of the form of friction present on the right-hand side of (2.8a). Perhaps a more sophisticated parameterization of the effects of inertia, as discussed by Hogg (1993), could be combined with the present model to yield more realistic results.

To investigate the role of inertia, we have constructed a model similar to the present model, using the large-scale semi-geostrophic equations of Salmon (1996). Results of numerical simulations (Shepherd, 1999) show that recirculating gyres form on both sides of the western boundary current as it flows across the slope. The southern gyre in the numerical model can be explained by JEBAR, but the northern gyre seems to require the presence of baroclinic eddies, in contrast to the present, noninertial theory.

Perhaps the most intriguing aspect of the solutions presented here is the existence of a maximum value of $\mathscr{T}$ ($\mathscr{T}_{\max}$, say) for which solutions of this structure exist. It remains an open question as to what happens when $\mathscr{T}$ exceeds this maximum value. As $\mathscr{T}$ approaches $\mathscr{T}_{\max}$, the subpolar gyre extends to the southwest equatorial corner in an increasingly thin region. At some small value of $(\mathscr{T}_{\max} - \mathscr{T})$, this region may become sufficiently thin that a different boundary-layer structure develops. Further work must be done to elucidate this structure, but numerical simulations (Shepherd, 1999) suggest that for $\mathscr{T} > \mathscr{T}_{\max}$, the gyres may not meet in the corner region $r = O(\nu^{1/3})$, but may instead meet on the western boundary at some region significantly to the north of the equator. Salmon and Ford (1995) suggest that a value of $\mathscr{T} = 5.0$ is appropriate for the North Atlantic, which exceeds the maximum value permitted by the present solutions. In that case, the present analysis is to be regarded as an essential first step in the general theory of (2.8), with further work required to obtain solutions for the larger values of $\mathscr{T}$ appropriate to the North Atlantic Ocean. Moreover, T will in general depend on latitude in the inflow regions at the edge of the slope, whereas in this paper we have considered only two uniform values of T in the deep ocean, so that in this paper all the effects of baroclinicity are concentrated in the thin baroclinic current. Perhaps solutions obtained for larger values of T, and with more general baroclinic structure, will resemble more closely the flow observed in the western North Atlantic than those presented here.

Acknowledgments. This paper is the result of several years of experiments with the planetary geostrophic equations. The work started while the author was a UCAR ocean modelling post-doctoral fellow. Computational equipment was provided by grant 16127 from the Royal Society of London. Numerous conversations with R. Salmon are gratefully acknowledged. I also thank T. Allen and G. Moore for helpful discussions and J. R. Shepherd, V. Kamenkovich and an anonymous reviewer for suggesting several improvements to the manuscript.

APPENDIX

A. Numerical solution of equation (3.5)

We solve (3.5) using a spectral method, in which Jacobi polynomials, rather than the more familiar trigonometric functions, are used as the basis. Writing $\mu = \sin\theta$, we have

$$\frac{1}{R(1-\mu^2)}\frac{\partial\psi_0}{\partial R} = \left(\frac{\partial^2}{\partial R^2} + \frac{1}{R}\frac{\partial}{\partial R} + \frac{\mu}{R^2}\frac{\partial}{\partial\mu} + \frac{1-\mu^2}{R^2}\frac{\partial^2}{\partial\mu^2}\right)\zeta_0, \tag{A.1a}$$

$$R(1-\mu^2)^{1/2}\zeta_0 = \left(\frac{\partial^2}{\partial R^2} + \frac{1-\mu^2}{R^2}\frac{\partial^2}{\partial\mu^2}\right)\psi_0. \tag{A.1b}$$

We now write

$$\psi_0 = \sum_{n=1}^{N} \psi_{2n+1}(r)p_{2n+1}(\mu), \tag{A.2a}$$

$$\zeta_0 = \sum_{n=1}^{N} \zeta_{2n+1}(r)p_{2n+1}(\mu), \tag{A.2b}$$

where $p_\alpha(\mu)$ is the Jacobi polynomial with both parameters equal to -1 (i.e. $p_\alpha(\mu) = P_\alpha^{(-1,-1)}(\mu)$ in the notation of Abramowitz and Stegun, 1964), and $p_\alpha(\mu)$ satisfies

$$(1-\mu^2)\frac{d^2p_\alpha}{d\mu^2} + \alpha(\alpha-1)p_\alpha = 0. \tag{A.3}$$

We require a sum over only odd-valued (i.e. odd-numbered) Jacobi polynomials, starting at $\alpha = 3$, because $\psi_0 = \zeta_0 = 0$ at $\mu = 0, 1$.

For odd values of $\alpha \geq 3$ and $\beta \geq 3$, the Jacobi polynomials satisfy the orthogonality relation

$$\int_0^1 \frac{p_\alpha(\mu)p_\beta(\mu)}{1-\mu^2}\,d\mu = 0 \qquad \text{if} \qquad \alpha \neq \beta, \tag{A.4}$$

where, as usual, the value of the integral when $\alpha = \beta$ depends upon the normalization.

We now substitute the expansions (A.2) into the equations (A.1), divide by (A.1b) by $(1-\mu^2)^{3/2}$, multiply by $p_\alpha(\mu)$ and integrate from $\mu = 0$ to $\mu = 1$. All the integrands are either bounded or have integrable singularities. The result is a system of matrix equations of the form

$$\frac{1}{R}\frac{d\psi_i}{dR} = A_{ij}\left(\frac{d^2\zeta_j}{dR^2} + \frac{1}{R}\frac{d\zeta_j}{dR} - \frac{j(j-1)}{R^2}\zeta_j\right) + \frac{B_{ij}}{R^2}\zeta_j, \tag{A.5a}$$

$$R\zeta_i = C_{ij}\left(\frac{d^2\psi_j}{dR^2} - \frac{j(j-1)}{R^2}\psi_j\right), \tag{A.5b}$$

where the matrices A_{ij} and B_{ij} are tri-diagonal, and C_{ij} is full, and the integers i and j run through odd values greater than one, and summation over the repeated index j is implied.

The radial derivatives in (A.5) are discretized using second-order centered differences. They are then solved for each Jacobi mode in turn as a two-by-two block tri-diagonal system, using an iterative method in which the off-diagonal terms for $j > i$ are evaluated using the values at the previous iteration. We have found that this relaxation typically converges in five to ten iterations.

Boundary conditions are $R \to \infty$ are matching conditions, in which $\zeta \to 0$ and $\psi \to \Psi[(\pi/2\lambda) \tan \theta]$. The solution shown in Figure 2 has $\psi_5 = -1$ and $\psi_i = 0$ for all other odd integers $i \geq 3$ and $\zeta_i = 0$ at $R = 100$.

B. The limit $\rho \to \infty$

In the limit $\rho \to \infty$ (i.e., the deep ocean) we have $\beta = 1$, $H = 1$, $\rho = x$, $dH/d\rho = 2/(\pi\lambda x^2)$. Then

$$c\xi_0(\rho) = \frac{\mathsf{T}}{4\pi}\int_{-\infty}^{\infty} dk \int_{\rho}^{\infty} d\rho' \frac{2}{\pi\lambda\rho'^2} \exp\{ik[\xi_0(\rho) - \xi_0(\rho)')] - k^4(\rho' - \rho)\}. \quad \text{(B.1)}$$

Then writing $\rho' = \rho x$ and $k' = \rho^{1/4}k$, we have

$$c\xi_0 = \rho^{-5/4}\frac{\mathsf{T}}{2\lambda\pi^2}\int_{-\infty}^{\infty} dk' \int_{1}^{\infty} dx x^{-2} \exp\{i\rho^{-1/4}k'[\xi_0(x) - \xi_0(x')] - (k')^4(x-1)\}. \quad \text{(B.2)}$$

It follows from (B.2) that $\xi_0(x) = O(x^{-5/4})$ as $\rho \to \infty$. The terms $ik[\xi_0(x) - \xi_0(x')]$ in (B.2) can then be neglected, and we obtain the following asymptotic form for $\xi_0(x)$ in the limit $x \to \infty$:

$$\begin{aligned}\xi_0 = \rho^{-5/4}\frac{\mathsf{T}}{2\lambda\pi^2 c}\int_{-\infty}^{\infty} dk' \int_{1}^{\infty} dx x^{-2} \exp\{-(k')^4(x-1)\} \\ = \rho^{-5/4}\frac{\mathsf{T}}{2\sqrt{2}\Gamma\left(\frac{3}{4}\right)\lambda\pi c}\int_{1}^{\infty}\frac{dx}{x^2(x-1)^{1/4}}.\end{aligned} \quad \text{(B.3)}$$

C. The limit $\rho \to -\infty$

In the limit $\rho \to -\infty$ (i.e. the corner region) we have

$$\begin{aligned}|\xi_0(\rho)| &= \frac{\mathsf{T}}{4\pi c}\int_{-\infty}^{\infty} dk \int_{\rho}^{\infty} d\rho' \frac{dH(\rho')}{d\rho'} \exp\{ik(\xi_0(\rho) - \xi_0(\rho') - k^4(\rho' - \rho)\} \\ &\leq \frac{\mathsf{T}}{4\pi c}\int_{\rho}^{\infty} d\rho' \frac{dH(\rho')}{d\rho'}\int_{-\infty}^{\infty} dk \exp\{-k^4(\rho' - \rho)\} \\ &= \frac{\mathsf{T}}{4\sqrt{2}\Gamma\left(\frac{3}{4}\right)c}\int_{\rho}^{\infty}\frac{dH(\rho')}{d\rho'}(\rho' - \rho)^{-1/4}\, d\rho'.\end{aligned} \quad \text{(C.1)}$$

This integral can be evaluated using standard asymptotic methods for the limit $\rho \to -\infty$. There are two asymptotic regions to consider, $\rho' = O(\rho)$ and $\rho' = O(1)$. The principal contribution comes from the region $\rho' = O(1)$, in which $(\rho' - \rho)^{-1/4}$ may be approximated by $(-\rho)^{-1/4}$. The result is

$$|\xi_0(\rho)| \le \frac{\mathsf{T}(-\rho)^{-1/4}}{4\sqrt{2}\Gamma\left(\frac{3}{4}\right)c}\int_0^1 dH = \frac{\mathsf{T}}{4\sqrt{2}\Gamma\left(\frac{3}{4}\right)c}(-\rho)^{-1/4}. \tag{C.2}$$

D. The region $r = O(\nu^{-1/3})$

If we examine the solution in the region $r = O(1)$, we see that, as $r \to \infty$, the thickness of the front is α^{-1}, where α is given by (5.4). As $r \to \infty$, we have

$$\frac{3}{2}\Psi'(y_0)\left(\frac{f}{H} - y_0\right)^2 = 1 - H \Rightarrow \frac{f}{H} - y_0 = \left[\frac{2}{3\Psi'(y_0)}(1 - H)\right]^{1/2}. \tag{D.1}$$

Now, as $x \to \infty$, we have $H = 1 - 2/(\pi\lambda x) + O(x^{-3})$. Thus $d(y/H)/ds = -\frac{1}{3}(2/\lambda\pi)^{1/2}x^{-3/2}\,(dx/ds)$. Now, in the deep ocean, we have $dx/ds = 1$, and so

$$\alpha = \left(-\frac{H}{\nu}\frac{d(y/H)}{ds}\right)^{1/3} = \left(\frac{2}{27\lambda\pi}\right)^{1/6}\nu^{-1/3}x^{-1/2} + O(x^{-3/2}). \tag{D.2}$$

Since this implies a frontal scale of infinite extent as $x \to \infty$, it is important to resolve this apparent contradiction for large x.

Let us start, then, by deriving the scaling for a "Stefan" region in $r \gg 1$. We first observe that the tangential coordinate s and normal coordinate n are to leading order x and y, respectively. Then, to obtain a balance between advection and diffusion in the momentum equation, we require

$$\frac{\psi}{s} \sim \frac{\nu\psi}{n^4}. \tag{D.3}$$

Integrating across the temperature jump, and recalling $(dH/ds) = O(s^{-2})$, we have

$$\frac{1}{s^2} \sim \frac{\nu\psi}{n^3}. \tag{D.4}$$

Taking these two together yields

$$s = O(\nu^{-1/3}) \qquad n = O(\nu^{1/6}) \qquad \psi = O(\nu^{1/6}). \tag{D.5}$$

The equation in the region $r = O(\nu^{-1/3})$ is then

$$-\frac{\partial\psi}{\partial s} - \frac{\mathscr{T}}{\lambda\pi}s^{-2}\delta(n - n_0(s)) = \frac{\partial^4\psi}{\partial n^4}, \tag{D.6}$$

with all variables re-scaled according to (D.5), and the solution-technique for this equation is identical to that given in Section B. It can be shown to match smoothly to the solution in the region $r = O(1)$.

E. The region $r = O(\nu^{1/7})$

As $r \to 0$, the path taken by the front will become parallel to a contour of y/H. The term $J(\psi, y/H)$ will then not be well-represented by $(-d(y/H)/ds)(\partial\psi/\partial n)$, as required to derive (5.2). To be precise, we have

$$-\frac{d(y/H)}{ds}\frac{\partial\psi}{\partial n} = O(\alpha), \tag{E.1}$$

where α is given by (5.4), while, for $H \approx 2\lambda x/\pi$

$$J(\psi, y/H) = \frac{2\lambda}{\pi}\frac{1}{r}\frac{\partial\psi}{\partial r}\sec^2\theta = O(r^{-2}), \tag{E.2}$$

and so the approximation $J(\psi, y/H) \approx (d(y/H)/ds)(\partial\psi/\partial n)$ required for (5.2) to hold breaks down when

$$\alpha = O(r^{-2}) \qquad \text{i.e.} \qquad r = O(\nu^{1/7}). \tag{E.3}$$

We can obtain equation for the region $r = O(\nu^{1/7})$ as follows. We write the equations using polar co-ordinates. As $r \to 0$, we have from Eq. (5.13) that θ must approach come constant value, Θ, say. Then we derive a scaling for $\Delta\theta \equiv \theta - \Theta$ by requiring a balance of terms in the momentum equation. This gives $\Delta\theta = O(\nu^{1/7})$.

We now write $\vartheta = \nu^{-1/7}(\theta - \Theta)$. Then the equation for ψ is

$$\frac{1}{\lambda}\sec^2\Theta\frac{\partial\psi}{\partial r} + \frac{\mathscr{T}}{2}\frac{\partial H}{\partial r}\delta(\vartheta - \vartheta_0(r)) = \frac{1}{r^3 H}\frac{\partial^4\psi}{\partial\vartheta^4}, \tag{E.4}$$

where here we have re-scaled r on $\nu^{1/7}$. In this region $(\partial H/\partial r) \approx 2\lambda\pi^{-1}\cos\Theta$, and the path $\vartheta = \vartheta_0(r)$ taken by the front must be determined as part of the solution. Thus, a full Stefan problem is recovered in this region.

Eq. (E.4) can be solved using techniques identical to those of Section 4. However, we have not solved Eq. (E.4), since it affects the solution only for small values of r; the solution in the region $r = O(\nu^{1/7})$ does not affect the leading-order solution in the region $r = O(1)$.

REFERENCES

Abramowitz, M. and I. A. Stegun. 1964. A Handbook of Mathematical Functions, Dover, NY 1046 pp.

Batchelor, G. K. 1956. On steady laminar flow with closed streamlines at large Reynolds numbers. J. Fluid Mech., *1*, 177–190.

Bryan, F. F., C. W. Böning and W. R. Holland. 1995. On the mid-latitude circulation in a high-resolution model of the North Atlantic. J. Phys. Oceanogr., *18,* 280–303.

Cane, M. A., V. M. Kamenkovich and A. Krupitsky. 1998. On the utility and disutility of JEBAR. J. Phys. Oceanogr, *28,* 519–526.

Crank, J. 1984. Free and Moving Boundary Problems, Oxford University Press. 425 pp.
Hogg, N. G. 1992. On the transport of the Gulf Stream between Cape Hatteras and the Grand Banks. Deep-Sea Res., *39,* 1231–1246.
—— 1993. Toward a parameterization of the eddy field near the Gulf Stream. Deep-Sea Res., *40,* 2359–2376.
Hogg, N. G., R. S. Pickart, R. M., Hendry and W. J. Smethie Jr. 1986. The Northern Recirculation Gyre of the Gulf Stream. Deep-Sea Res., *33,* 1139–1165.
Holland, W. R. 1967. On the wind-driven circulation in an ocean with bottom topography. Tellus, *19,* 582–599.
—— 1973. Baroclinic and topographic influences on the transport in western boundary currents. Geophys. Fluid Dyn., *4,* 187–210.
Johns, W. E., T. J. Shay, J. M. Bane and D. R. Watts. 1995. Gulf Stream structure, transport and recirculation near 68°W. J. Geophys. Res., *100,* 817–838.
Leaman, K., E. Johns and T. Rossby. 1989. The average distribution of volume transport and potential vorticity with temperature at three sections across the Gulf Stream. J. Phys. Oceanogr., *19,* 36–61.
Liu, Z. Y. 1990. On the influence of the continental-slope on the western boundary-layer—the enhanced transport and recirculation. J. Mar. Res., *48,* 255–285.
Munk, W. H. 1950. On the wind-driven ocean circulation. J. Meteor., *7,* 79–93.
Myers, P. G., A. F. Fanning and A. J. Weaver. 1996. JEBAR, bottom pressure torque and Gulf Stream separation. J. Phys. Oceanogr., *26,* 671–683.
Olbers, D. and C. Wübber. 1991. The role of wind and buoyancy forcing of the Antarctic Circumpolar Current, Technical Report 22, Alfred-Wegener-Institutfür Polar-und Meeresforschung.
Özgökmen, T. M., E. P. Chassignet and A. M. Paiva. 1997. Impact of wind forcing, bottom topography and inertia on midlatitude jet separation in a quasigeostrophic model. J. Phys. Oceanogr., *27,* 2460–2476.
Robinson A. and H. Stommel. 1959. The oceanic thermocline and the associated thermohaline circulation. Tellus, *11,* 295–308.
Salmon, R. 1992. A two-layer Gulf Stream over a continental slope. J. Mar. Res., *50,* 341–365.
—— 1994. Generalized two-layer models of ocean circulation. J. Mar. Res., *52,* 865–908.
—— 1996. Large-scale semigeostrophic equations for use in ocean circulation models. J. Fluid Mech., *318,* 85–105.
Salmon, R. and R. Ford. 1995. A simple model of the joint effect of baroclinicity and relief. J. Mar. Res., *53,* 211–230.
Sarkisyan, A. S. and V. F. Ivanov. 1971. Joint effect of baroclinicity and bottom relief as an important factor in the dynamics of sea currents. Bull. Acad. Sci. USSR Atmos. and Ocean Phys., *7,* 173–178.
Schmitz, W. J. Jr. and M. S. McCartney. 1993. On the North Atlantic circulation. Rev. Geophys., *31,* 29–49.
Shepherd, J. R. 1999. Modelling Ocean Circulation with the Large-Scale Semi-Geostrophic Equations, PhD Thesis, University of London.
Slater, L. J. 1966. Generalized Hypergeometric Functions, Cambridge University Press, 273 pp.
Stommel, H. 1948. The westward intensification of wind-driven ocean currents. Trans. Am. Geophys. Union, *29,* 202–206.
Thompson, L. 1995. The effect of continental rises on the wind-driven ocean circulation. J. Phys. Oceanogr., *25,* 1296–1316.
Welander, P. 1968. Wind-driven circulation in one- and two-layer oceans of variable depth. Tellus, *20,* 1–15.

Received: *21 October, 1999;* revised: *13 March, 2000.*